BRNO UNIVERSITY OF TECHNOLOGY
VYSOKÉ UČENÍ TECHNICKÉ V BRNĚ

FACULTY OF MECHANICAL ENGINEERING
FAKULTA STROJNÍHO INŽENÝRSTVÍ

INSTITUTE OF SOLID MECHANICS, MECHATRONICS AND BIOMECHANICS
ÚSTAV MECHANIKY TĚLES, MECHATRONIKY A BIOMECHANIKY

A COMPARATIVE STUDY OF ULTIMATE LOAD AND STIFFNESS OF METAL-TO-COMPOSITE JOINTS
SROVNÁVACÍ STUDIE ÚNOSNOSTI A TUHOSTI VYBRANÝCH SPOJŮ KOVOVÉ A KOMPOZITNÍ ČÁSTI KONSTRUKCE

MASTER'S THESIS
DIPLOMOVÁ PRÁCE

AUTHOR Bc. Michal Tchír
AUTOR PRÁCE

SUPERVISOR prof. RNDr. Ing. Jan Vrbka, DrSc., dr. h. c.
VEDOUCÍ PRÁCE

BRNO 2016

BRNO UNIVERSITY OF TECHNOLOGY FACULTY OF MECHANICAL ENGINEERING

Master's Thesis Assignment

Institut:	Institute of Solid Mechanics, Mechatronics and Biomechanics
Student:	**Bc. Michal Tchír**
Degree programm:	Applied Sciences in Engineering
Branch:	Engineering Mechanics and Biomechanics
Supervisor:	**prof. RNDr. Ing. Jan Vrbka, DrSc., dr. h. c.**
Academic year:	2015/16

As provided for by the Act No. 111/98 Coll. on higher education institutions and the BUT Study and Examination Regulations, the director of the Institute hereby assigns the following topic of Master's Thesis:

A comparative study of ultimate load and stiffness of metal-to-composite joints

Brief description:

Computational modelling of ultimate load and stiffness at the joint area between metalic and composite part of the deformation loaded combined construction making use of the Finite Element Method (FEM). Formulation of the apropriate computational model with the emphasis on the binding of both used materials. Comparison of several joint variants and evaluation of results.

Master's Thesis goals:

Computational assesment of ultimatate load and stifness of selected joints between metalic and composite part of the deformationally loaded combined construction using the Finite Element Method (FEM). These joints are widely applicated in the aircraft structures. Formulation of the apropriate computational model. Computational assesment of ultimate load will be compared with experimental results. Comparison of several construction variants and evaluation of results.

Bibliography:

Jones,R.M.: Mechanics of composite materials. Hemisphere Publishing Corpopration. New York, 1975

Vrbka,J.: Mechanika kompozitů. Ústav mechaniky těles, mechatroniky a biomechaniky, FSI VUT v Brně, Brno, 2008

Niu,C.Y.M.: Composite airframe structure. Conmilit Press Ltd., Hong Kong, 2005

Middleton,D.H.: Composite materiál in aircraft structure. Longman Singapore Publisher Ltd., 1990

Madenci,E.,Guven,I.: The finite element method and applications in engineering using ANSYS. Springer, 2006

Students are required to submit the thesis within the deadlines stated in the schedule of the academic year 2015/16.

In Brno, 30. 11. 2015

L.S.

VYSOKÉ UČENÍ TECHNICKÉ V BRNĚ FAKULTA STROJNÍHO INŽENÝRSTVÍ DĚKANÁT

prof. Ing. Jindřich Petruška, CSc.	doc. Ing. Jaroslav Katolický, Ph.D.
Director of the Institute	FME Dean

Abstract

Nowadays, one of the method for joining especially thick and highly loaded composite components is mechanically fastened bolted joint which allows disassembly of components e.g. for repair unlike adhesively bonded joint. Traditional sizing method is first-ply-failure, however prediction post first-ply-failure behavior is important too. For structural analysis of the joints as well as for other components is widely used the finite element method. Since modern nonlinear solvers have capability for investigation post first-ply-failure behavior of laminate, this capability of one of them was used in this thesis for investigation of mechanical behavior of laminate made of GFRP layers which was joined to aluminium bracket using bolts. Progressive damage finite element models of two metal-to-composite joints were built in order to determine post first-ply-failure behaviour using three different failure criteria - maximum stress, Hill and Tsai-Wu using Nastran solver. Force-displacement curves, stiffness-displacement curves and values of loads at ultimate displacement were compared with experimental data. As residual stiffness factor influences the results of progressive failure analysis, sensitivity studies of the factor were done, in which accuracy and achieving convergence were investigated. In the case of the first joint an agreement is less satisfying, however, the agreement in the case of the second joint, which has a thin steel reinforcing plate on its bottom side, is considerably better. Excellent agreement is especially with interactive criteria Hill and Tsai-Wu.

Key Words

progressive failure analysis, first ply failure, failure criteria, bolted joints, the finite element method, composite, laminate, orthotropic material, damage

Abstrakt

V současnosti jedna z metod spojování zejména tlustých a vysoce zatížených kompozitních komponent je šroubový spoj, který je možné rozebrat pro případ opravy na rozdíl od lepeného spoje. Kompozitní konstrukce se tradičně dimenzují tak, aby během provozu nedošlo k porušení první vrstvy laminátu, nicméně důležité je taky poznat chování laminátu po porušení první vrstvy. Pro strukturální analýzu nejenom spojů, ale také dalších komponent se používá metoda konečných prvků a protože moderní nelineání řešiče jsou schopné modelovat chování laminátu po porušení první vrstvy, tato schopnost jednoho z nich byla využita v této práci při zkoumaní chování sklolaminátu spojeného s hliníkovou částí šrouby. Konečno-prvkové modely dvou spojů kovové a kompozitní části konstrukce schopné popsat progresivní porušování laminátu byly postaveny s využitím tří různých poruchových kritérií – kritéria maximálního napětí, kritéria Hill a kritéria Tsai-Wu. Problém byl řešen s využitím řešiče Nastran. Křivky síla-posuv, tuhost-posuv a hodnoty zatížení při hraničním posuvu byly porovnány s výsledky experimentů. Jelikož faktor zbytkové tuhosti ovlivňuje výsledky analýzy progresivního porušování, byly provedeny citlivostní studie zkoumajíci vliv faktoru na přesnost a stabilitu výpočtu. Shoda výpočtu s experimentem v případe prvního šroubového spoje je méně uspokojivá, nicméně shoda v případě druhého spoje, který má zesilující tenkou ocelovou destičku na spodní straně, je podstatně lepší. Výborná shoda je zejména při použití interaktivních kritérií Hill a Tsai-Wu.

Klíčová slova

analýza porušování laminátů, porušení první vrstvy, poruchová kritéria, šroubové spoje, metóda konečných prvků, kompozit, laminát, ortotropní materiál, poškození

Bibliographic citation

TCHIR, M. *A comparative study of ultimate load and stiffness of metal-to-composite joints.* Brno: Brno university of technology, Faculty of mechanical engineering, 2016. 76 pages. Supervisor: prof. RNDr. Ing. Jan Vrbka, DrSc., dr. h. c.

Declaration of originality

I hereby declare that the master's thesis on the topic *A comparative study of ultimate load and stiffness of metal-to-composite joints* I wrote independly using literature and sources written in the list in the attachment of this thesis.

In Brno 26 May 2016 .....

Acknowledgement

I would like to express gratitude to my supervisor prof. RNDr. Ing. Jan Vrbka, DrSc., dr. h. c. for giving me oportunity to work on this interesting topic, his optimism and useful recommendations, which improved quality of the thesis. I would like to thank my consultant, Ing. Petr Vosynek, Ph.D., for encouraging me to pursue the topic, for helpfulness and for professional managing the work on the thesis. I would like to express my gratitude to M.Sc. Volodymyr Symonov, my consultant at Institute of aerospace engineering, for introducing me to the world of composite materials, willingness to answer my questions and a permission to use results of his work in this thesis. I am grateful to prof. Ing. Přemysl Janíček, DrSc., FEng. for helpful discussion and inspirational advices, which helped to clearify solution of the problem investigated in this work.

Especially I am grateful to my parents, who have supported me during whole my studies.

Thank you.

Contents

Introduction 12
1 Problem situation 13
1.1 Formulation of the problem 13
1.2 Objectives of the thesis 13
1.3 Type of the problem 13
2 System of important quantities 15
3 Joints 16
3.1 Type 1 16
3.2 Type 2 17
3.3 Failure of bolted joints 17
4 Research study 19
5 Mechanics of composite materials 21
5.1 Constitutive equations for an orthotropic material 21
5.2 Failure theories 23
5.2.1 Maximum stress theory 23
5.2.2 Energy based interaction theory (Tsai-Hill) 25
5.2.3 Interactive tensor polynomial theory (Tsai-Wu) 26
5.3 Progressive composite failure 27
5.4 Strengh ratio 28
6 Solution method 30
6.1 The finite element method 30
6.2 Nonlinear solution 32
6.3 Continuum mechanics 33
7 Description of computional models and settings of solution 35
7.1 Geometry 36
7.2 Mesh 38
7.2.1 Mesh sensitivity study 38
7.3 Model of material 39
7.3.1 Sensitivity study of residual stiffness factor 41
7.4 Model of boundary conditions 42
7.5 Contacts 43
7.6 Model of loads 46

7.7 Setting of the solution 48
8 Results 49
8.1 Type 1 50
8.1.1 Comparison of force-displacement curves and stiffness-displacement curves 50
8.1.2 Displacement and failure index using maximum stress failure criterion 51
8.1.3 Displacement and failure index using Hill failure criterion 52
8.1.4 Displacement and failure index using Tsai-Wu failure criterion* 53
8.2 Type 2 54
8.2.1 Comparison of force-displacement curves and stiffness-displacement curves 54
8.2.2 Displacement and failure index using the maximum stress failure criterion 55
8.2.3 Displacement and failure index using the Hill failure criterion 56
8.2.4 Displacement and failure index using the Tsai-Wu failure criterion* 57
8.3 Comparison of Type 1 and Type 2 58
8.3.1 Evaluation of loads at ultimate displacement 59
9 Discussion 62
10 Conclusion 65
List of symbols 70
List of abreviations and names of software 72
List of figures 73
List of tables 76

Introduction

Since 1970s the use of fiber composites in aircraft structures has increased and the main reason is the significant weight-saving and other advantages that these composites can provide. Nevertheless, the high cost of composites compared with similar structures made from metal, mainly aluminium alloys, do not allow their use on every aircraft structural component. Apart from the high cost, composites have long range of disadvantages, low resistance to mechanical damage, low through-thickness strength and temperature limitations are only the most important.[7] Engineers need to achieve the levels of safety given by norms, laws and standards and these days, the finite element method is widely used for determination stresses and strains in materials, hence for ensurance the safety in a development phase of a product. Several sizing methods for composite structures have developed over the last 40 years. One of the most important method is first-ply failure which is often acceptable to sign off a drawing. However, progressive failure analysis allows to describe the post first-ply-failure behavior of a structure. Nowadays, engineers use progressive failure analyses for better understanding of the structure, increasing realiability and saving costs. In this thesis progressive failure analyses using the finite element method of metal-to-composite bolted joints are described.

Fig. 1 Airbus A350XWB has fuselage and wings made of CFRP. [32]

1 Problem situation

According to Janíček [1]:

„A problem situation is a nonstandard situation unlike a standard situation, because different activities than routine, known or algorithmizable have to be used for a solution. “

Since the use of fiber composites in aircraft structures is increasing, therefore a need of an effective joining exists and one of the method of joining especially thick composite components is use of bolted joints. Traditional sizing method of composites is first-ply-failure analysis, but the FPF may lead to very conservative sizing, therefore engineers and scientists are interested in post first-ply-failure behavior of material these days. Other reasons can be increasing realiability and safety of structure.

1.1 Formulation of the problem

Investigation of post first-ply-failure behavior of two bolted joints with emphasis on laminate using three different failure criteria by the finite element method and comparison of results from finite element analyses with experimental data.

1.2 Objectives of the thesis

„An objective is a statement formulated by a subject about an intention to do or to create something, where an impulse for the intention comes from the subject or its surround. [1]*“*

The aim of the thesis is computational modelling of post first-ply-failure behavior of selected metal-to-composite joints with emphasis on laminate. Objectives, which should be done, are described below:

- to build a computational models of the joints involved geometry models, material models with three different failure criteria, model of boundary conditions and loads,
- to do progressive failure analyses of the joints with respective failure criteria,
- to determine force-displacement curves, stiffness-displacement curves and ultimate loads if possible,
- to compare the results of finite element analyses with experimental data,
- to evaluate the results.

1.3 Type of the problem

Since the problem has technical character, knowledge of mechanics of materials, continuum mechanics, mathematics and materials is needed – the problem is multidisciplinary.

In adition, the problem is causal, because the bindings to the enviroment are known as well as its geometry and activation. The problem is direct because the inputs are known. However, outputs, that had been measured, are known too, which can help to asses the results of progressive failure analysis. Geometry, boundary conditions, material characteristics are given, and the aim is to determine force-displacement curves, stiffness-displacement curves, and ultimate load if possible.

According to Janíček [9], an experiment has five utilizations:

- reduction experiment
- verification experiment
- formulational experiment
- experiment for concretization
- experiment for identification

In this work the experimental data will be used for determination of loads at ultimate displacement and for verification of results of the progressive failure analyses.

2 System of important quantities

As the system of important quantities helps to sort out the quatities and clarify a solution of the problem, the system was written below. [1].

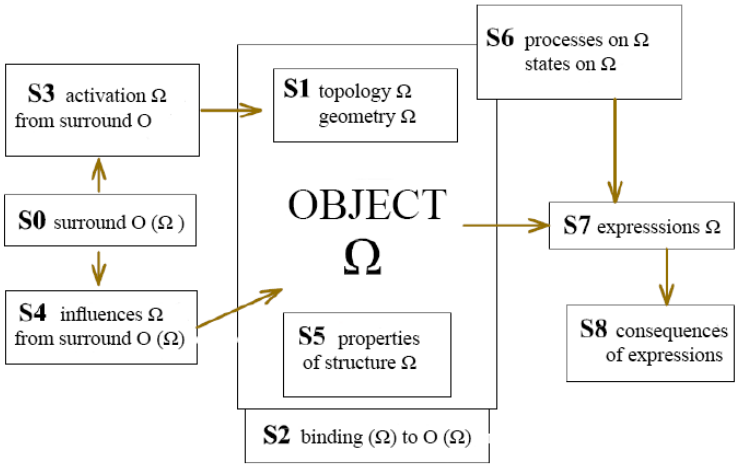

Fig. 2 Schematics of the system of important quantities.[12]

In this case the bolted metal-to-composite joint is the object Ω and the problem is to do a progressive failure analysis of the joint and to determine force, displacement, stiffness, and ultimate load.

Next, the following aspects of the system were determined:

- **S0** Temperature and humidity.
- **S1** Geometries of the joints Type 1 and 2.
- **S2** Binding of the models of the joints will be modelled using boundary conditions.
- **S3** In a first step bolt preload will be applied, in the next step deformational load will be used.
- **S4** Since temperature and humidity were constant, they were omitted.
- **S5** Mechanical properties of the laminated plate, the bracket, the bolt and the reinforcement.
- **S6** Stress-strain states of the joints.
- **S7** Outputs of the analyses are displacements, stresses and constraint forces.
- **S8** In the category consequences of expressions are included failure indeces, safety factors, strength ratios, and design ultimate loads.

3 Joints

Due the facts written in the Introduction, a combination of common materials like metals and composites is getting more popular and as a result of the combination of materials, the need of effective joining exists. According to Baker [7], three categories of joint types are used: mechanically fastened joints using bolts and rivets, adhesively bonded joints using a polymeric adhesive and a combination of mechanical fastening and adhesive bonding. Intuitively, it may be concluded that mechanical fastening is an unsatisfactory means of joining composites because the fastener holes must cut fibers, destroying part of the load path. However, since considerable loss in strength occurs (typically to half of the original strength), the only feasible or economic use of bolted joints is joining highly loaded thick composite components.[7] Nevertheless, according to Heimbs, Schmeer, Blaurock and Steeger [18] "*The use of carbon fibre-reinforced plastic materials for primary aircraft structures is ever expanding in the last decades with the fuselage of the latest generation of large commercial aircraft, i.e. Airbus A350XWB and Boeing 787, being built with this composite material. Despite considerable progress in adhesive bonding technologies, the connection of composite structural elements is still mainly based on mechanically fastened bolted joints, allowing for component disassembly e.g. for repair.*"

3.1 Type 1

First joint consists of laminated plated, made of 16 plies, a bracket made of aluminium alloy D16, two steel bolts M5 (grade 12.9) and two steel nuts. A material of the layers is glass fiber reinforcement polymer.

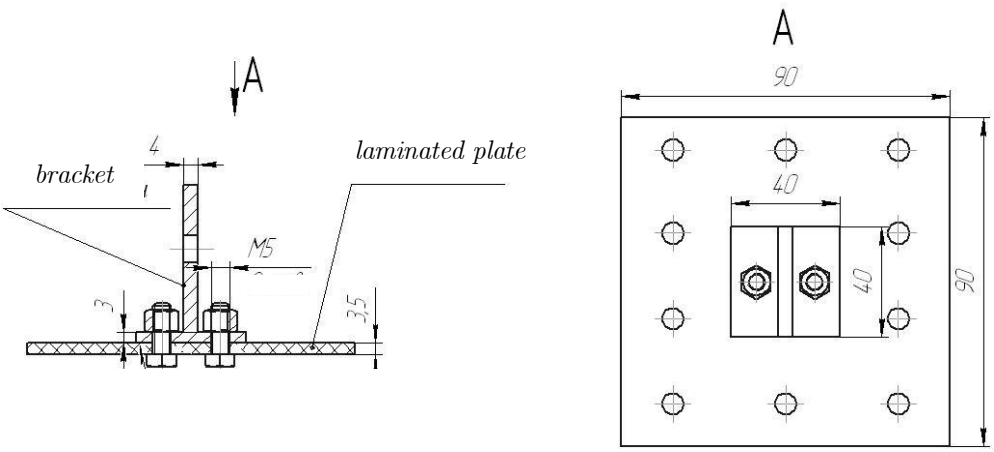

Fig. 3 Technical drawing of the joint Type 1.

3.2 Type 2

Second joint similarly like the joint Type 1 consists of laminated plated, made of 16 plies, a bracket made of aluminium alloy D16, two bolts M5 (grade 12.9), two nuts and, in adition, a steel reinforcement on the bottom of the plate as shown in **Fig. 4**. The material of the layers is same as in the case of Type 1.

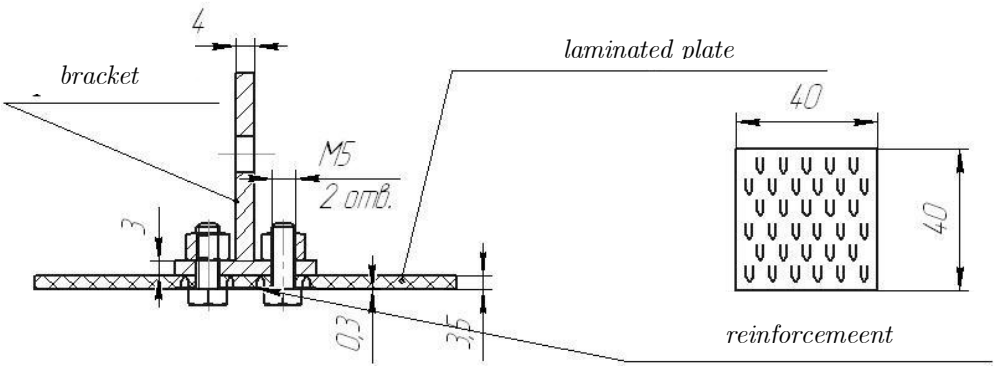

Fig. 4 Technical drawing of the joint Type 2.

3.3 Failure of bolted joints

According to Baker [7], main failure modes in mechanical joints in composites include net-tension failure, cleavage tension, essentially mixed tension/shear; bolt-head pulling through the laminate, a problem particularly with deeply countersunk holes; and bolt failure due to bearing failure.

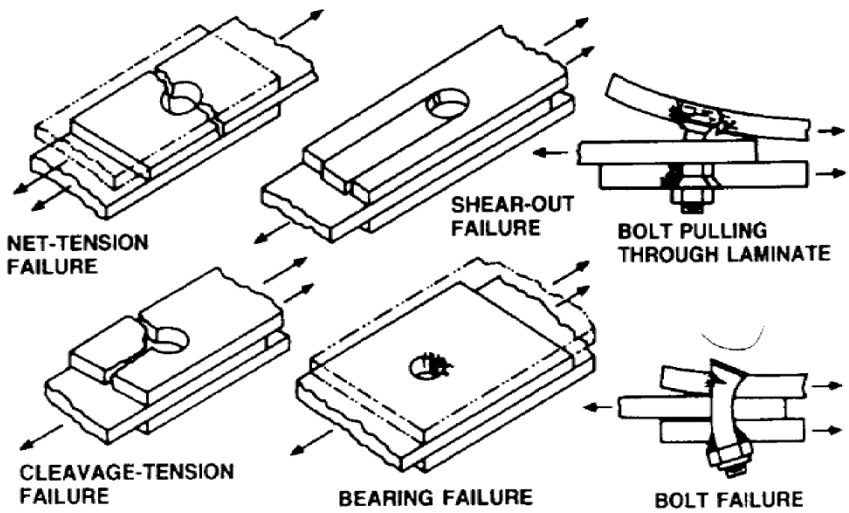

Fig. 5 Schematic illustration of main failure modes in mechanical joints in composites.[15]

The joints Type 1 and Type 2 were tested at the Institute of aerospace engineeering at Brno university of technology and the laminated plates in **Fig. 6** and **Fig. 7** show the failure mode „bolt pulling through laminate“ displayed above in **Fig. 5**. The research was focused mainly on laminate.

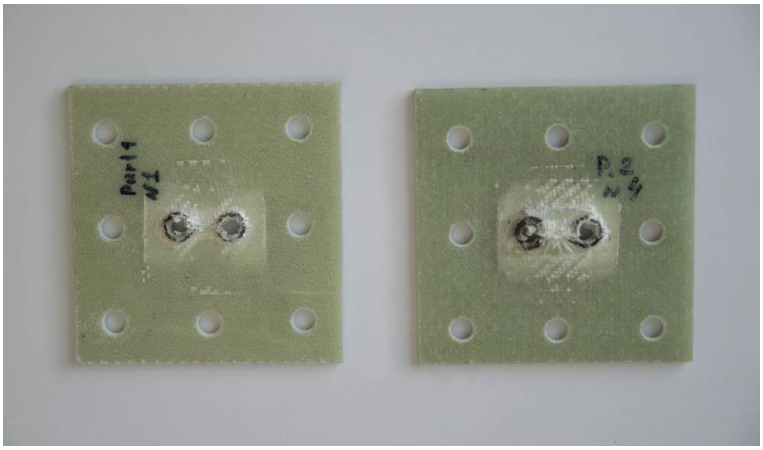

Fig. 6 Top side of laminated plates of the joints after the measurement; on the left Type 1, on the right Type 2. Published with permission of Institute of aerospace engineering of Brno university of technology.

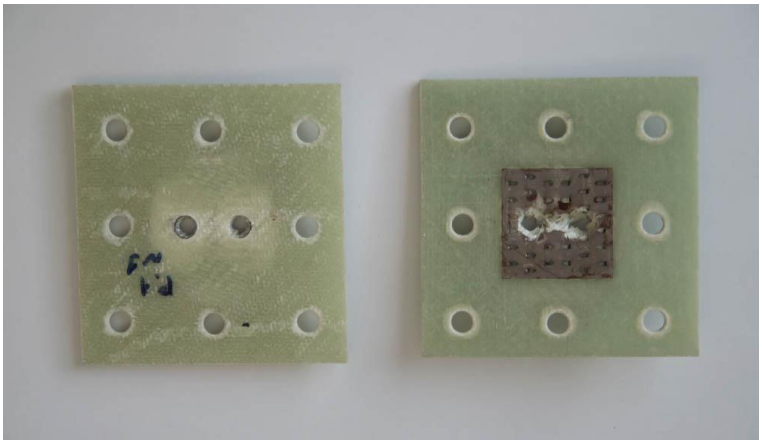

Fig. 7 Bottom side of laminated plates of the joints after the measurement; on the left Type 1, on the right Type 2. Published with permission of Institute of aerospace engineering of Brno university of technology.

4 Research study

A progressive failure of bolted joints using the finite element method has been researched along with an increasing of performace of computers and a progress in building of composite structures.

Adam, Bouvet, Castanié, Daidié and Bonhomme in [17] the pull-through phenomenon firstly studied by simplified circular pull-through test method. The research extended the Discrete Ply Model Method developed by Bouvet et al., where cohesive elements were placed at the interfaces between solid elements to represent matrix cracks and delamination, thus allowing the natural coupling between two damage modes. The model showed good correalation with test results in terms of load-displacement curves and prediction of the damage map until failure. Heimbs, Schmeer, Blaurock and Steeger in 18] conducted test series of mechanically bolted joints with countersunk head in quasi-isotropic carbon-epoxy composite laminate under quasi-static and dynamic loads with velocities up to 10 m/s. The test campaign covered bolt pull-through tests, single lap shear tests with one and two bolts and coach peel tests. No rate sensitivity occurred for majority of test configurations, only the single lap shear tests with bolts showed a change of failure mode at the highest test velocity enabling highest energy absorption. Kabche, Caccese, Berube and Bragg in [19] presented an investigation of the structural performance of hybrid composite-to-metal bolted joints loaded in flexure, where the main goal was to develop a watertight, hybrid connection to resist bending loads. Use of dobler plates and foam inserts in a bolted joint resulted in higher strength and stiffness and can effectively mitigate joint opening, which improves the ability to seal the joint and maintain watertight integrity. Kelly and Hagström in [20] investigated experimentally and numerically a behavior of composites laminates subjected to transverse load. Damage was found to initiate at low load levels, typically 20-30 % of the failure load. The dominant initial failure mode was matrix intralaminar shear failure which occurred in sub-surface plies. The results from the finite element model were found to be in general agreement with experimental observations. Catalanotti, Camanho, Ghys and Marques in [21] presented an experimental and numerical study of the fastener pull-through failure mode in flass-fiber reinforced plastic laminates using both phenolic and vinylester resins. There is shown that the type of resin does not affect the mechanical response of the joint when a pull-through test is performed because similar values of the subcritical initial and final failure loads were obtained. The prediction of the sub-critical initial failure load was performed using three-dimensional finite element model where cohesive elements were used to simulate delamination, because it was observed that the main failure mechanism was the delamination. Elder, Verdaasdonk and Thomson in [2218] considered the capability of finite element modelling to predict fastener pull-through failure of composite laminates, which is dominated by inter-ply delamination and through-thickness shear failure of the laminate. They used the LS-DYNA software for the study and found out that the use of simplified FE models does have merit in modelling fastener pull-through provided the material quasi-isotropic and the boundary conditions are uniform around a

circular perimeter. Stocchi, Robinson and Thomson [23] dealt with analysis of single lap shear composite joint with countersunk fasteners under static tensile load. In the analysis he studied the influence of clamping force, coefficient of friction and clearance on the joint behavior and fount that the model is able to identify correctly the joint critical locations. Camanho and Matthews [24] studied a joint behavior of single and multi-fastener joints in order to predict failure. He concluded that "there is no general method that should be used to predict failure, but progressive damage models are quite promising since important aspect of joint's behavior can be modelled using this approach." Moreover, he claims that "the use of three-dimensional models is suggested with appropriate three-dimensional failure criterion and property degradation law." C. T. McCarthy with M. A. McCarthy in [25] analysed a 3D progressive damage finite element model of multi-bolt, double-lap composite joints developed in the non-linear finite element code Abaqus." They studied the effects of variable bolt-hole clearance and found out that clearance can cause major changes in the load distribution and damage mechanism in the joint and it can lead to a significant reduction in the load at which initial failure occurs. Wang, Zhou, Wu and Zhou [26] used extended finite element method (XFEM) to predict failure of single-lap bolted joint. Hühne, Zerbst, Kuhlman and Rolfes in [27] investigated a structural behavior of a single-lap, single-bolt composite joint using three-dimensional finite element model and in contrast to previous investigations, a influence of a liquid shim layer added between two laminates on structural behavior of the joints was studied. As a first approach was used Hashin three-dimensional failure criterion and a constant degradation model and it led to very convervative results after validation with experimental data. As a second approach they improved the model using a continuos degradation model and discover very good correlation with the experimental data. Mouritz [28] reviewed published research into polymer composite laminates reinforced in the through-thickness direction with z-pin. In the paper research into the manufacture, microstructure, delamination resistance, damage tolerance, joint strength and mechanical properties of z-pinnned composites is described. Z-pinning can improve interlaminar toughness, impact damage resistance, post-impact damage tolerance and through-thickness properties. The paper also describes the adverse effects of z-pins on the in-plane mechanical properties.

According to the papers can be claimed the following:

- no general method exists that should be used to predict failure, but progressive damage models are quite promising since important aspect of joint's behavior can be modelled using this approach,
- the type of resin does not affect the mechanical response of the joint when a pull-through test is performed,
- Z-pinning can improve interlaminar toughness, impact damage resistance, post-impact damage tolerance and through-thickness properties,
- negative effects of z-pins are reduced elastic modulus, strength and fatigue performance;
- mechanical properties of laminate with z-pins depend on size and locations of the pins.

5 Mechanics of composite materials

The most used materials these days are isotropic and homogeneus material (steel, aluminium alloys etc). In contrast, due to increase in reliability and decrease of cost, composite materials are used more and more. Composite materials are usually inhomogeneus and nonisotropic (orthotropic, anisotropic) unlike metals. An orthotropic material can be described as a material with three different properties in three perpendicular directions.[6]

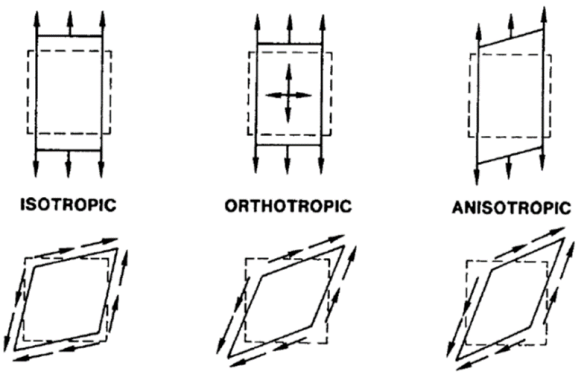

Fig. 8 Comparison of behaviour of isotropic, orthotropic and anisotropic material. [6]

5.1 Constitutive equations for an orthotropic material

Hooke's law for linear elastic orthotropic material can be described as

$$\begin{bmatrix} \sigma_1 \\ \sigma_2 \\ \sigma_3 \\ \tau_{23} \\ \tau_{31} \\ \tau_{12} \end{bmatrix} = \begin{bmatrix} C_{11} & C_{12} & C_{13} & 0 & 0 & 0 \\ C_{21} & C_{22} & C_{23} & 0 & 0 & 0 \\ C_{31} & C_{33} & C_{33} & 0 & 0 & 0 \\ 0 & 0 & 0 & C_{44} & 0 & 0 \\ 0 & 0 & 0 & 0 & C_{55} & 0 \\ 0 & 0 & 0 & 0 & 0 & C_{66} \end{bmatrix} \cdot \begin{bmatrix} \varepsilon_1 \\ \varepsilon_2 \\ \varepsilon_3 \\ \gamma_{23} \\ \gamma_{31} \\ \gamma_{12} \end{bmatrix} \tag{5.1}$$

where σ_i...component of normal stress, where $i = 1, 2, 3$

τ_{ij}...component of shear stress, where i, j and $i, j = 1, 2, 3$

ε_i...component of normal strain, where $i = 1, 2, 3$

γ_{ij}... component of shear strain, where i, j and $i, j = 1, 2, 3$

C_{ij}...component of stiffness matrix $\boldsymbol{C}$, where $i, j = 1, 2, 3, 4, 5, 6$

Inverse Hooke's law for linear elastic orthotropic material is given by

$$\begin{bmatrix} \varepsilon_{11} \\ \varepsilon_{22} \\ \varepsilon_{33} \\ \gamma_{23} \\ \gamma_{31} \\ \gamma_{12} \end{bmatrix} = \begin{bmatrix} S_{11} & S_{12} & S_{13} & 0 & 0 & 0 \\ S_{21} & S_{22} & S_{23} & 0 & 0 & 0 \\ S_{31} & S_{33} & S_{33} & 0 & 0 & 0 \\ 0 & 0 & 0 & S_{44} & 0 & 0 \\ 0 & 0 & 0 & 0 & S_{55} & 0 \\ 0 & 0 & 0 & 0 & 0 & S_{66} \end{bmatrix} \cdot \begin{bmatrix} \sigma_{11} \\ \sigma_{22} \\ \sigma_{33} \\ \tau_{23} \\ \tau_{31} \\ \tau_{12} \end{bmatrix}$$

where S_{ij}...component of compliance matrix $\boldsymbol{S}$, where i, j = 1, 2, 3, 4, 5, 6. (5.2)

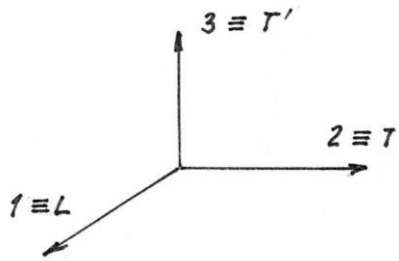

Fig. 9 The base othotropic cooordinate system.[2]

Normal strains and shear strains in principal orthotropic directions are [10]

$$\varepsilon_1 = \frac{\sigma_1}{E_1} - \nu_{21} \cdot \frac{\sigma_2}{E_2} - \nu_{31} \cdot \frac{\sigma_3}{E_3} \tag{5.3}$$

$$\varepsilon_2 = \frac{\sigma_2}{E_2} - \nu_{32} \cdot \frac{\sigma_3}{E_3} - \nu_{12} \cdot \frac{\sigma_1}{E_1} \tag{5.4}$$

$$\varepsilon_3 = \frac{\sigma_3}{E_3} - \nu_{13} \cdot \frac{\sigma_1}{E_1} - \nu_{23} \cdot \frac{\sigma_2}{E_2} \tag{5.5}$$

$$\gamma_{23} = \frac{\tau_{23}}{G_{23}} \tag{5.6}$$

$$\gamma_{31} = \frac{\tau_{31}}{G_{31}} \tag{5.7}$$

$$\gamma_{12} = \frac{\tau_{12}}{G_{12}} \tag{5.8}$$

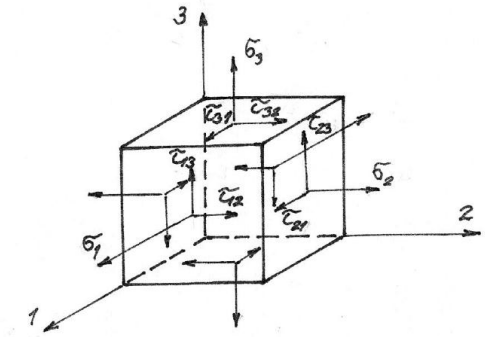

Fig. 10 Loaded element of orthotropic material in principal orthotropic directions. [2]

The equations (5.3) — (5.8) can be written in matrix form

$$\begin{bmatrix} \varepsilon_1 \\ \varepsilon_2 \\ \varepsilon_3 \\ \gamma_{23} \\ \gamma_{31} \\ \gamma_{12} \end{bmatrix} = \begin{bmatrix} \frac{1}{E_1} & -\frac{\nu_{21}}{E_2} & \frac{\nu_{31}}{E_3} & 0 & 0 & 0 \\ -\frac{\nu_{21}}{E_2} & \frac{1}{E_1} & -\frac{\nu_{21}}{E_2} & 0 & 0 & 0 \\ -\frac{\nu_{21}}{E_2} & -\frac{\nu_{21}}{E_2} & \frac{1}{E_1} & 0 & 0 & 0 \\ 0 & 0 & 0 & \frac{1}{G_{23}} & 0 & 0 \\ 0 & 0 & 0 & 0 & \frac{1}{G_{31}} & 0 \\ 0 & 0 & 0 & 0 & 0 & \frac{1}{G_{12}} \end{bmatrix} \cdot \begin{bmatrix} \sigma_1 \\ \sigma_2 \\ \sigma_3 \\ \tau_{23} \\ \tau_{31} \\ \tau_{12} \end{bmatrix} \tag{5.9}$$

From symmetry condition for compliance matrix $\boldsymbol{S}$ results the equation between material contants

$$\frac{\nu_{ij}}{E_i} = \frac{\nu_{ji}}{E_j} \tag{5.1}$$

where $i \neq j, and\ i, j = 1, 2, 3$. [2]

5.2 Failure theories

5.2.1 Maximum stress theory

The maximum stress theory was adapted to composites under plane stress conditions, where the off-axis strength of a unidirectional lamina is a function of fiber orientation by three different curves corresponding to three different failure modes.

According to the maximum stress theory, failure occurs when at least one stress component along one of the principal material axes exceeds the corresponding along the principal material axes and planes (σ_1, σ_2, σ_3, τ_4, τ_5, τ_6), and the failure condition is expressed in the form of the following subcriteria [3]

$$\sigma_1 = \begin{cases} F_{1t} & \text{when} \quad \text{for } \sigma_1 > 0 \\ -F_{1c} & \text{when} \quad \text{for } \sigma_1 < 0 \end{cases} \tag{5.2}$$

$$\sigma_2 = \begin{cases} F_{2t} & \text{when} \quad \text{for } \sigma_2 > 0 \\ -F_{2c} & \text{when} \quad \text{for } \sigma_2 < 0 \end{cases} \tag{5.10}$$

$$\sigma_3 = \begin{cases} F_{3t} & \text{when} \quad \text{for } \sigma_3 > 0 \\ -F_{3c} & \text{when} \quad \text{for } \sigma_3 < 0 \end{cases} \tag{5.11}$$

$$|\tau_4| = F_4 \tag{5.12}$$

$$|\tau_5| = F_5 \tag{5.13}$$

$$|\tau_6| = F_6 \tag{5.14}$$

For material with transverse isotropy on the 2-3 plane,

$$F_{2t} = F_{3t} \tag{5.15}$$

$$F_{2c} = F_{3t} \tag{5.16}$$

$$F_5 = F_6 \tag{5.17}$$

where F_i ....ultimate stress of a lamina along i direction, where $i = 1, 2, 3, 4, 5, 6$.

As shown in **Fig. 11**, for a two dimensional state of stress with τ_6, the failure envelope have the form of a rectangle.[3]

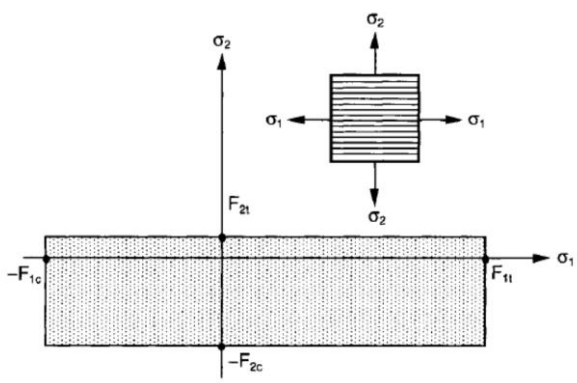

Fig. 11 Failure envelope for unidirectional lamina under biaxial normal loading (maximum stress theory). [3]

5.2.2 Energy based interaction theory (Tsai-Hill)

The deviatoric or distortional energy has been proposed by many investigators (e.g., von Mises, Hencky, Nadai, Novozhilov) in various forms as a failure criterion for isotropic ductile metals. For a two-dimensional state of stress referred to the principal stress directions, the von Mises yield criterion has the form [3]

$$\sigma_1^2 + \sigma_1^2 - \sigma_1\sigma_2 = \sigma_{yp}^2 \tag{5.18}$$

where σ_{yp} is the yield stress.

The following criterion for ductile metals with anisotropy was proposed by Hill

$$A\sigma_1^2 + B\sigma_1^2 - C\sigma_1\sigma_2 + D\tau_6^2 = 1 \tag{5.19}$$

where A, B, C, and D are material parameters characteristic of the current state of anisotropy.

For uniaxial longitudinal loading to failure, $\sigma_2^u = F_1$, $\sigma_2 = \tau_6 = 0$ and the equation above yields

$$A = \frac{1}{F_1^2} \tag{5.20}$$

For uniaxial transverse loading to failure, $\sigma_2^u = F_2$, $\sigma_1 = \tau_6 = 0$ and the equation (5.19) yields

$$B = \frac{1}{F_2^2} \tag{5.21}$$

For in-plane shear loading to failure, $\sigma_1 = \sigma_2 = 0$, $\tau_6^u = F_6$ and the equation (5.19)

$$D = \frac{1}{F_6^2} \tag{5.22}$$

The superscript u in the above denotes the ultimate value of stress at failure. Since failure will occur when the transverse stress σ_2 reaches the transverse strength value F_2, which is much lower than the longitudinal strength F_1, the equation (5.19) then yields [3]

$$C = -\frac{1}{F_1^2} \tag{5.23}$$

The Tsai-Hill criterion for a two-dimensional state of stress is given by substituting A, B, C and D into (5.19)

$$\frac{\sigma_1^2}{F_1^2} + \frac{\sigma_2^2}{F_2^2} + \frac{\tau_6^2}{F_6^2} - \frac{\sigma_1\sigma_2}{F_1^2} = 1 \tag{5.24}$$

The appropriate strength values can be used in the equation above according to the signs of the normal stresses σ_1 and σ_2, because there is no distinction between tensile and compressive strengths, hence

$$F_1 = \begin{cases} F_{1t} & \text{when} \quad \sigma_1 > 0 \\ F_{1c} & \text{when} \quad \sigma_1 > 0 \end{cases} \tag{5.25}$$

$$F_2 = \begin{cases} F_{2t} & \text{when} \quad \sigma_2 > 0 \\ F_{2c} & \text{when} \quad \sigma_2 > 0 \end{cases} \tag{5.26}$$

As $F_2 \approx F_3$ and $F_5 \approx F_6$, the failure criterion for three-dimensional state of stress is

$$\frac{\sigma_1^2}{F_1^2} + \frac{\sigma_2^2 + \sigma_3^2}{F_2^2} + \frac{\tau_4^2}{F_4^2} + \frac{\tau_5^2 + \tau_6^2}{F_5^2} - \frac{\sigma_1\sigma_2}{F_4^2} - \frac{\sigma_1\sigma_2}{F_4^2} = 1 \tag{5.27}$$

or

$$\frac{\sigma_1^2 - \sigma_1\sigma_2 - \sigma_1\sigma_3}{F_1^2} + \frac{\sigma_2^2 + \sigma_3^2 - \sigma_2\sigma_3}{F_1^2} + \frac{\tau_4^2}{F_4^2} + \frac{\tau_5^2 + \tau_6^2}{F_5^2} = 1 \tag{5.28}$$

The theory is based on Hill's theory, which is suitable for homogeneous, anisotropic and ductile material, however, composites are mostly heterogeneous and brittle.

5.2.3 Interactive tensor polynomial theory (Tsai-Wu)

Tsai and Wu [3][16] developed a modified tensor polynomial theory by assuming the existence of a failure surface in expanded form

$$\begin{aligned} f_1\sigma_1 + f_2\sigma_2 + f_3\sigma_3 + f_4\tau_4 + f_5\tau_5 + f_6\tau_6 + f_{11}\sigma_1^2 + f_{22}\sigma_2^2 + f_{33}\sigma_3^2 \\ + f_{44}\tau_4^2 + \\ + f_{55}\tau_5^2 + f_{66}\tau_6^2 + 2f_{12}\sigma_2 + 2f_{13}\sigma_3 + 2f_{14}\tau_4 + 2f_{15}\tau_5 + 2f_{16}\tau_6 \\ + 2f_{23}\sigma_2\sigma_3 + \\ + 2f_{24}\sigma_2\tau_4 + 2f_{25}\sigma_2\tau_5 + 2f_{36}\sigma_3\tau_6 + 2f_{45}\tau_4\tau_5 + 2f_{46}\tau_4\tau_6 + 2f_{56}\tau_5\tau_6 \\ = 1 \end{aligned} \tag{5.29}$$

where f_i, f_{ij} are second order and fourth strength tensors, and $i, j = 1, 2, \ldots, 6$. [3]

All linear terms in the shear stresses and all terms associated with interaction of normal and shear stresses and between shear stresses acting on different planes are omitted, because the shear strength of a unidirectional composite, F_4, F_5 and F_6 reffered to the principal material planes ar independant of the sign of the shear stress (τ_4, τ_5, τ_6). [3]

$$\begin{aligned} -f_4 = f_5 = f_6 = f_{14} = f_{15} = f_{16} = f_{24} = f_{25} = f_{26} = f_{34} = f_{35} = f_{36} \\ = f_{45} = \\ = f_{46} = f_{56} = 0 \end{aligned} \tag{5.30}$$

If transverse isotropy in the 2-3 plane is assumed, the number of coefficient is reduced,

$$f_2 = f_3 \quad f_{22} = f_{33} \quad f_{55} = f_{66} \quad f_{12} = f_{13} \tag{5.31}$$

thus the criterion can be written as

$$f_1\sigma_1 + f_2(\sigma_2 + \sigma_2) + f_{11}\sigma_1^2 + f_{22}(\sigma_2^2 + \sigma_3^2) + f_{44}\,\tau_4^2 + f_{66}(\,\tau_5^2 + \,\tau_6^2) + 2f_{12}(\sigma_1\sigma_2 + \sigma_1\sigma_3) + 2f_{23}\sigma_2\sigma_3 = 1 \tag{5.32}$$

$$f_1\sigma_1^2 + f_2\sigma_2^2 + f_{11}\sigma_1^2 + f_{22}\sigma_2^2 + f_{22}\,\tau_6^2 + 2f_{12}\sigma_1\sigma_2 = 1 \tag{5.33}$$

After several mathematical operations, which are described in the detail in [3], the Tsai-Wu criterion can be reduced to

$$\sigma_1^2 + \sigma_2^2 + \sigma_3^2 - \sigma_1\sigma_2 - \sigma_2\sigma_3 - \sigma_3\sigma_1 + 3(\tau_4^2 + \tau_5^2 + \tau_6^2) = {F_{index}}^2 \tag{5.34}$$

where F_{index} is the uniaxial strength and the equation (5.34) is the widely used failure criterion for isotropic material (Huber-Mises-Hencky).

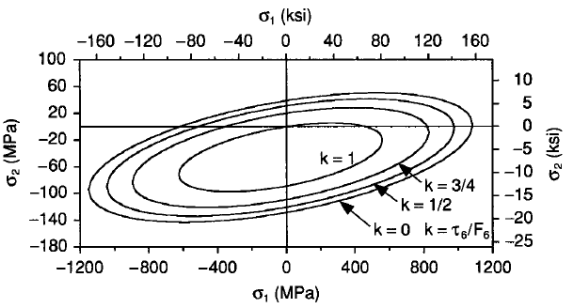

Fig. 12 Failure envelopes for unidirectional E-glass/epoxy lamina under biaxial loading with different levels of shear stress (Tsai-Wu criterion). [3]

5.3 Progressive composite failure

According to MSC Nastran 2014 Nonlinear User's Guide [13]

"Model 1 – Selective Gradual Degradation

This model uses a selective degradation of the moduli depending on failure mode. The moduli are decreased gradually when failure occurs. Within an increment, it attempts to keep the highest failure index less than or equal to one. Whenever a failure index F larger than one occurs, stiffness reduction factors r_i are calculated based upon the value of the failure indices. The incremental contribution to the total reduction factor is calculated as

$$\Delta r_i = -(1 - e^{1-F_{index}}) \tag{5.35}$$

where Δr_i is the incremental contribution to the total reduction factor,

F_{index} is failure index.

This is done differently for different failure criteria as described below. Six such reduction factors are stored and updated. They are then used for scaling the respective material modulus according to

$$E_{11}^{new} = r_1 E_{11}^{orig} \tag{5.36}$$

$$E_{22}^{new} = r_2 E_{22}^{orig} \tag{5.37}$$

$$E_{33}^{new} = r_3 E_{33}^{orig} \tag{5.38}$$

$$G_{12}^{new} = r_4 G_{12}^{orig} \tag{5.39}$$

$$G_{23}^{new} = r_5 G_{23}^{orig} \tag{5.40}$$

$$G_{31}^{new} = r_6 G_{31}^{orig} \tag{5.41}$$

The Poisson's ratios are scaled in the same way as the corresponding shear modulus. For the maximum stress and maximum strain criteria the reduction factors are calculated separately from each separate failure index: r_1 is calculated from the first failure index as given by equation (5.36) *above, r_2 is calculated from the second failure index from equation* (5.37) *etc. Thus, there is no coupling of the different failure modes for these criteria. For the failure criteria which only have one failure index: Tsai-Wu, Hoffman and Hill, all six reduction factors are decreased in the same way, using the smallest of the r_i.*" [13]

5.4 Strengh ratio

Since failure indices F_{index} are in general nonlinear functions (except for the maximum stress and strain failure theories), thus they do not determine how far is to failure and hence strength ratio is a better indicator. Strength ratio SR is similar to margin of safety and is described using equation

$$SR = \frac{\text{allowable loads}}{\text{actual loads}}. \tag{5.42}$$

Table 1 Comparison of failure index and strength ratio.

Indicator	**Failure condition**
Failure index	$F_{index} > 1$
Strength ratio	$SR < 1$

For example, the determination of strength ratio will be showed using Tsai-Wu criteria.

$$F_{index} = \frac{\sigma_1^2}{X_T X_c} + \frac{\sigma_2^2}{Y_T Y_c} + 2F_{12}\sigma_1\sigma_2 + \frac{\tau_{12}^2}{S^2} + \sigma_1\left[\frac{1}{X_T} - \frac{1}{X_C}\right] + \sigma_2\left[\frac{1}{Y_T} - \frac{1}{Y_c}\right] \tag{5.43}$$

Actual stresses were substituted with the product $(SR \cdot actuall\ stress)$ and set $F_{index} = 1$, thus the equation will be

$$0 = \left[\frac{\sigma_1^2}{X_T X_c} + \frac{\sigma_2^2}{Y_T Y_c} + 2F_{12}\sigma_1\sigma_2 + \frac{\tau_{12}^2}{S^2}\right] SR^2 + \left[\sigma_1\left[\frac{1}{X_T} - \frac{1}{X_C}\right] + \sigma_2\left[\frac{1}{Y_T} - \frac{1}{Y_c}\right]\right] SR - 1 \tag{5.44}$$

As the equation (5.44) is quadratic, strength ratio will be determined solving for roots SR. [31]

When at certain failure index $F_{index} = 19{,}2287$ is strength ratio $SR = 0{,}228$, this indicates that the load is too high by a factor of

$$\frac{1}{SR} = \frac{1}{0{,}228} = 4{,}39 \tag{5.45}$$

Allowable load can be obtained dividing actual load by 4,39 or multiplying by strength ratio $SR = 0{,}228$. [31]

6 Solution method

6.1 The finite element method

The finite element method provides numerical solution of field problems. An essence of the method consists of a dividing a structure into finite number of elements, which are connected using nodes. The process of dividing the structure is called discretization. Degrees of freedom, defined in nodes, are refered to as unknown parameters. A functional dependence between the unknown parameters in the elements and nodes is given by a basis function. This greatly simplifies the mathematical description of complex shapes and replaces it with a description of basic geometric shapes such as rectangles, triangles or quads. This replaces the job search function continuous determination of the final number of unknown parameters to the search function interpolation. This treatment is called continuous to discrete problem. Discrete problem is then solved by means of algebraic finite number of steps using computer technology. Basic approaches to solving the system of equations can be divided according to several criteria. In terms of mathematical description of the problem distinguish the approaches to the differential and variation. Differential approach is to build a system of differential equations. Variational approach based on the observation that the processes occurring in nature have such a story, that of all the opportunities that may arise, to implement processes are minimized. The principle of this approach, therefore, is to find the functions for which it becomes functional a stationary value. Variational approach is referred to as energy and is used primarily in conjunction with numerical methods and FEM. When implementing the solution, it is possible to use either analytical or numerical solutions. If the task is solved analytically, the aim of finding a solution in the form of continuous functions using the methods of mathematical analysis. Numerical solution lies in continuous to discrete problem, as described in a previous paragraphs, and the solution of algebraic equations. Nowadays, the use of FEM as a numerical method in most cases carried out using variational formulation and deformation approach. The primary unknown functions are functions of displacements. [4]

The deformation variant of FEM is the Lagrange variational principle: *Only functions which give a stationary value of total potential energy Π are realized of all functions of displacements preserving continuity of body and meeting the geometric boundary conditions."* It is proven that the stationary value exists and its minimum is the functional Π.
Equation (6.1) expresses the total potential energy Π as difference of stress energy W and the potential of the external load P. [4]

$$\Pi = W - P \tag{6.1}$$

The strain energy of the body Ω is given by equation

$$W = \frac{1}{2}\int_{\Omega} \boldsymbol{\sigma}^T \epsilon \, dV \tag{6.2}$$

and the potential energy of the external load P

$$P = \int_{\Omega} \boldsymbol{u}^T \boldsymbol{o} \, dV + \int_{\Gamma_p} \boldsymbol{u}^T \boldsymbol{p} \, dS \tag{6.3}$$

In this relationship the following column matrices are used

- displacements $\boldsymbol{u}^T = [u, v, w]$ (6.4)
- strains $\boldsymbol{\epsilon}^T = [\epsilon_x, \epsilon_y, \epsilon_z, \gamma_{xy}, \gamma_{yz}, \gamma_{zx}]$ (6.5)
- stresses $\boldsymbol{\sigma}^T = [\sigma_x, \sigma_y, \sigma_z, \tau_{xy}, \tau_{yz}, \tau_{zx}]$ (6.6)
- distributed body forces $\boldsymbol{u}^T = [o_x, o_y, o_z]$ (6.7)
- surface forces $\boldsymbol{p}^T = [p_x, p_y, p_z]$ (6.8)

After substituting the global stiffness matrix, the total strain energy can be expressed as follows [4]:

$$W = \frac{1}{2}\boldsymbol{U}^T \boldsymbol{K}_1 \boldsymbol{U} \tag{6.9}$$

Similarly, after the representation of the overall matrix $\boldsymbol{F}$, the external load leads to:

$$\boldsymbol{P} = \boldsymbol{U}^T \boldsymbol{F} \tag{6.10}$$

Substituting equation (6.9) and (6.10) in equation for the total potential energy Π (6.11), we obtain

$$\Pi = \frac{1}{2}\boldsymbol{U}^T \boldsymbol{K} \boldsymbol{U} - \boldsymbol{U}^T \boldsymbol{F} \tag{6.11}$$

The stationary value of the functional Π according to the Lagrange variational principle:

$$\frac{\partial \Pi}{\partial \boldsymbol{U}} = 0 \tag{6.12}$$

Finally, from the partial derivatives according to u_1, u_2, u_3, u_4 we obtain a system of linear equations [4]:

$$\boldsymbol{KU} = \boldsymbol{F} \tag{6.13}$$

This equation is called the basic equation of the finite element method.

6.2 Nonlinear solution

In general, three causes of nonlinear behaviour exist

a) large displacements – a change of geometrical configuration during loading
b) material nonlinearity - plasticity, viscous behaviour
c) contact – a change of touching area. [30]

In NASTRAN Implicit Nonlinear software an algorithm of modified Newton-Raphson method is used. An essence of the algorithm is to divide total loading in every load step into substeps, so the loading increases gradually according to a current convergence rate. [30]

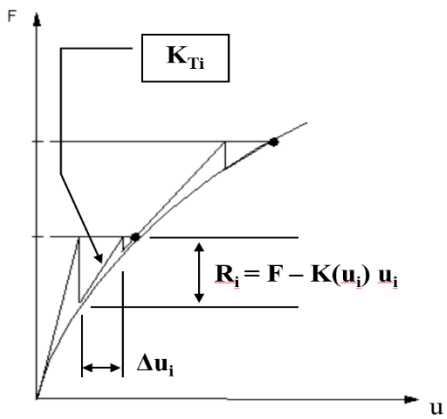

Fig. 13 Graphical representation of Newton-Raphson iterative solution. [30]

Each iteration is solving a linear system of equations for the displacement increment $\boldsymbol{\Delta u_i}$

$$\boldsymbol{K_{Ti}\Delta u_i} = \boldsymbol{F} - \boldsymbol{K(u_i)u_i}, \tag{6.14}$$

where $\boldsymbol{K_{Ti}}$ is immediate stiffness matrix (tangential to the curve F) and $\boldsymbol{F} - \boldsymbol{K(u_i)u_i}$ describes residual $\boldsymbol{R_i}$ of immediate external loading and internal body forces. Iterational process is ended if convergence criteria checking the value of residual forces to total loading are met [30]

$$\frac{R_i}{F_{total}} \leq \delta_F \tag{6.15}$$

Similarly, the value of displacement increment can be checked

$$\frac{\Delta u_i}{u_{total}} \leq \delta_u \tag{6.16}$$

compared with the given tolerances δ_F, δ_u. [30]

6.3 Continuum mechanics

Nowadays, two types of description of the motion of a continuum are mostly used:

1. Referential description, where the position X of the particle in a chosen reference configuration and the time are independant variables. The description is called the **Lagrangian description** when the reference configuration is chosen to bet he actual initial state at $t = 0$. The unstressed state is usually chosen to be the reference configuration.
2. Relative description, where the present position x and occupied by the particle at time t and the present time t are independent variables. The description is most used in fluid mechanics, sometimes calles the **Eulerian description**.[5]

Lagrangian description can be written symbolically

$$x = x(X, t) \tag{6.17}$$

with Cartesian components

$$x_r = x_r(X_1, X_2, X_3, t) \tag{6.18}$$

where X_1, X_2, X_3 are the material cooordinates of the particle.[5]

For determination stresses and strains at nonlinear analyses the following stress and stress tensor are used.

Green-Lagrange strain tensor is related to underformed coordinates but rotation of the element is respected. [29]

$$E_{ij}^L = \frac{1}{2}\left[\frac{\partial u_i}{\partial X_j} + \frac{\partial u_j}{\partial X_i} + \frac{\partial u_k}{\partial X_j}\frac{\partial u_k}{\partial X_i}\right] \tag{6.19}$$

Almansi-Hamel strain tensor is related to undeformed coordinates.[29]

$$E_{ij}^{A} = \frac{1}{2}\left[\frac{\partial u_i}{\partial x_j} + \frac{\partial u_j}{\partial x_i} - \frac{\partial u_k}{\partial x_j}\frac{\partial u_k}{\partial x_i}\right] \tag{6.20}$$

Cauchy logarithmic strain tensor uses the infinitesimal increment and current length unlike Green-Lagrange and Almansi-Hamel strain tensor. [29]

$$E_i^C = \int_{X_{i0}}^{x_{ik}} \frac{dx_i}{x_i} = \ln x|_{X_{i0}}^{x_{ik}} = \ln x_{ik} - \ln X_{i0} = \ln\left(\frac{x_{ik}}{X_{i0}}\right) = \ln \lambda_i \tag{6.21}$$

Cauchy stress tensor (Euler's stress tensor, true stress) is given by the derivation of a true elementary force and a true deformed area of an element.[29]

$$\sigma_i = \frac{dF_i}{dx_j dx_k} \tag{6.22}$$

The first Piola-Kirchhoff stress tensor (Lagrange stress tensor, engineering stress) is given by the derivation of a the true elementary force and undeformed area of the element.[29]

$$\tau_i = \frac{dF_i}{dX_j dX_k} \tag{6.23}$$

The second Piola-Kirchhoff stress tensor is given by the derivation of an elementery force dF_{0i} and undeformed area of an element. The tensor is without exact physical meaning, but i tis symmetric energy conjucated with Green-Lagrange strain tensor for large strains. The force dF_{0i} is changed at loading of an element unlike the true force in the same way as the elementary coordinate, which is changing according the following equation [29]

$$dx_i = \frac{dx_i}{dX_j} dX_j \tag{6.24}$$

For backward transformation to undeformed state the next formula is used

$$dx_i = \frac{dx_i}{dX_j} dX_j \tag{6.25}$$

Finally, the stress is defined as

$$dS_i = \frac{dF_{0i}}{dX_j dX_j} \tag{6.26}$$

7 Description of computional models and settings of solution

All major solvers like Abaqus, Ansys and MSC Nastran and Marc allow the progressive failure analysis of composite materials. Explicit solvers can be used too, but duration of the analyses especially with solid elements can take extremely long time. One of the most popular solvers these days, Abaqus, has programmed one failure criterion Hashin, wich can be used only with shell and continuum shell elements. Since the use of Hashin criterion with 3D solid elements is not available using GUI, a user has to write Abaqus user-defined material model UMAT (Abaqus Standard) or VUMAT (Abaqus Explicit), where the criterion will be included. The progressive failure analysis introduced in Ansys 14.0, has been extended in the following versions. Ansys has written the failure criteria and they can be used with solid 3D elements as well as with shell elements. In MAPDL, input and post – processing must be performed via commands, no GUI input is available. In Workbench, material input and post-processing is available, and the damage evolution law – continuum damage mechanics was finally added in version 17.0. Similarly as Ansys, Nastran Implicit Nonlinear as well as Marc have programmed several failure criteria, which can be used with solid 3D elements as well as with shell elements.

Several trial analysis were done using implicit solver Ansys, implicit solver Abaqus Standard, implicit solver Nastran SOL400 and explicit solver Abaqus Explicit. The trial analysis using explicit solver Abaqus Explicit was done with medium complex computional model with 4 elements through-thickness of the laminate, where solution of time 0,0002 s of total time 1 s using quad core Intel Xeon 3,6 GHz processor lasted unacceptable long time, thus the run was terminated. Explicit solver takes into account density of material, hence the kinetic energy of the deformed material should not exceed 5 % of its internal energy because the experiments were quasi-static, and it leads to long computation time. After discussion with my consultant at Institute of aerospace engineering at Brno university of technology, the solver Nastran Implicit Nonlinear SOL 400 was chosen for the FE analyses. The reasons for choosing Nastran were the following: acceptable computation times compared to explicit solver, availability at Institute of aerospace engineering, the fact that Nastran has programmed several failure criteria, which can be used for progressive failure analysis and the fact that it is widely used for aircraft development.

Table 2 Comparison of capabilities of implicit and explicit solver.

property	**nonlinear solver type**	
	implicit	explicit
post first-ply-failure behavior	yes	yes
prediction of ultimate load	depends on geometry, mesh and material model	yes
duration of analysis	normal	enormous

7.1 Geometry

Due to two planes of symmetry, only one-quarter geometries of the joints were created as shown in **Fig. 14**. The models (**Fig. 15** and **Fig. 16**) were built and cut for pure hexahedral meshing using the CAD system Solidworks and exported in STEP format. Afterwards, the geometries were imported to Patran for further processing of the models. Since according to Mouritz [28] affects especially interlaminar properties, which were not investigated in this work, z-pins of Type 2 were not modelled.

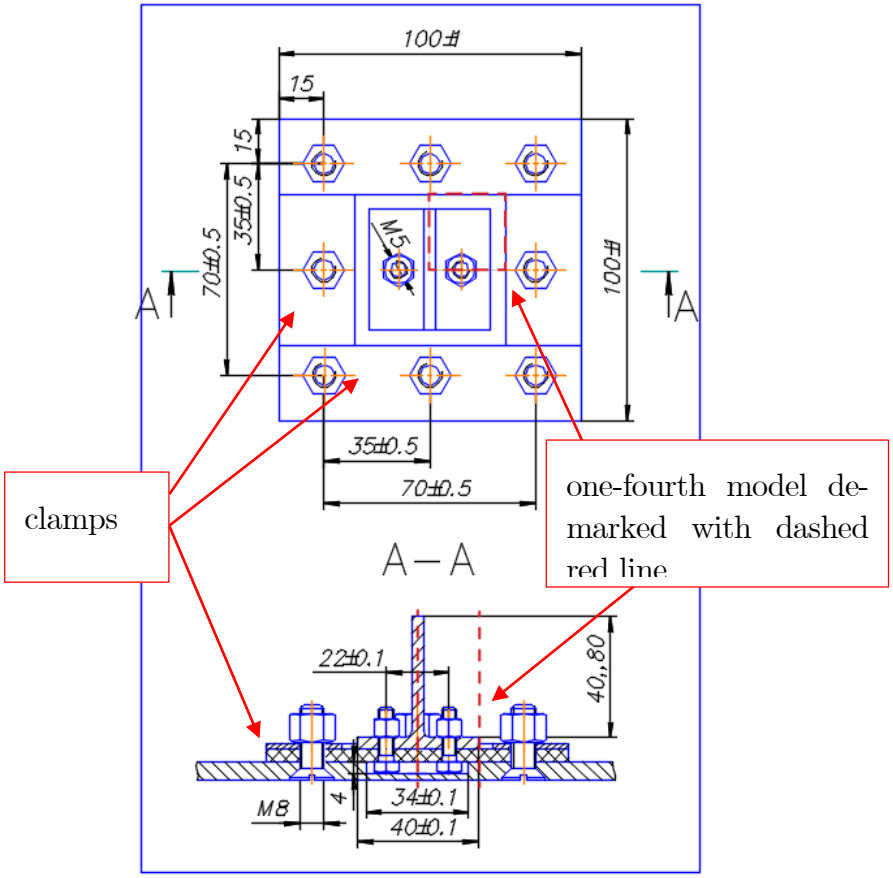

Fig. 14 Technical drawing of the joint Type1 clamped using the clamps for measurement, with red dashed lines demarked one fourth of joint, which was used for the computional models; same claping systém was used for testing the joint Type 2.

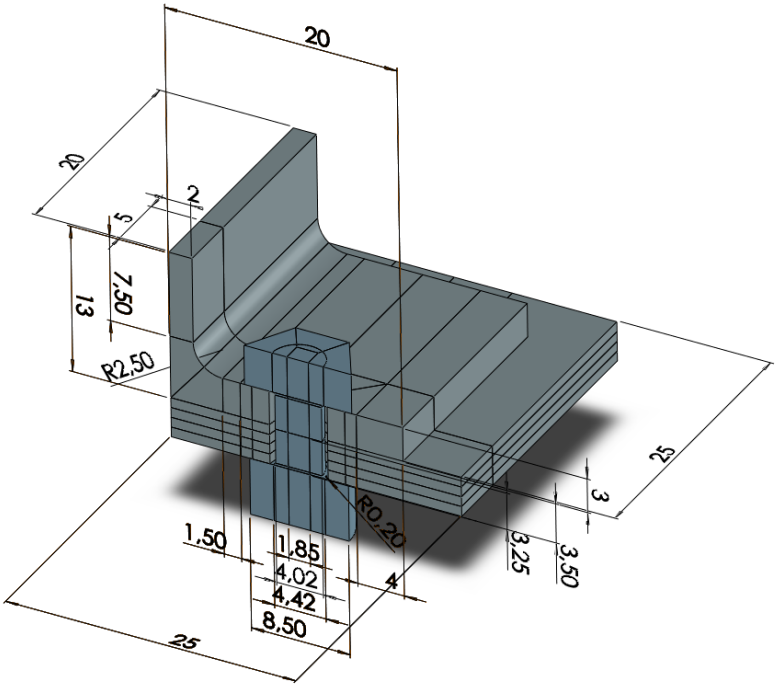

Fig. 15 Geometry of the computional model Type 1.

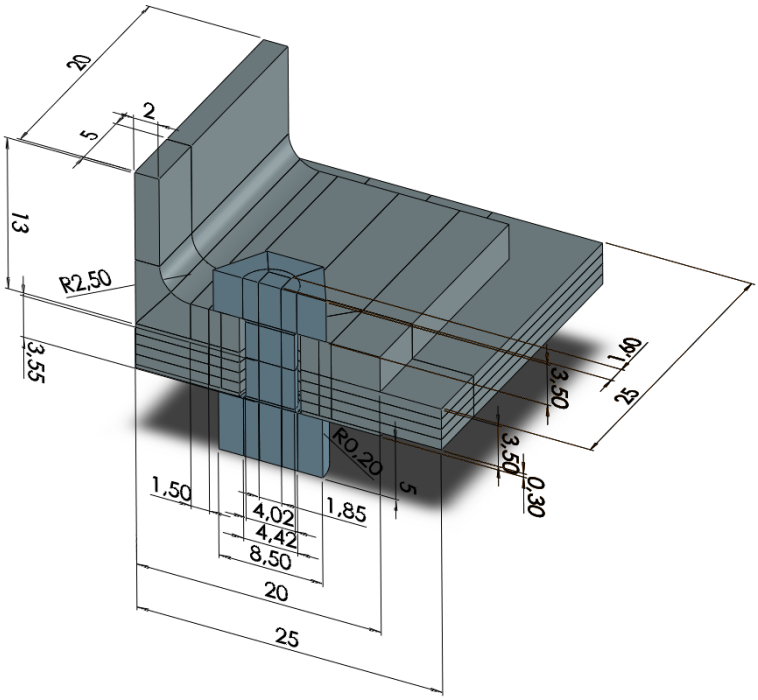

Fig. 16 Geometry of the computional model Type 2.

7.2 Mesh

7.2.1 Mesh sensitivity study

Using Patran several computational models of the Type 1 were made, each with different size of element. Since pure hexahedral mesh allows meshing the geometry model with lower number of the nodes, and the lower number of the nodes leads to shorter computional time, the assemblies of the joints were meshed with linear 8-node Nastran CHEXA elements. Moreover, the mesh sensitivity studies were done for better accuracy as shown in **Table 3**. The mesh had been refined in the four steps, and locations with highest values of Von Mises stress were refined after each run. The model was loaded using force 100 N on top surface of the bracket using Nastran RBE2 element, which constrained all degrees of freedom of respective nodes. Von Mises stress was chosen as a good indicator because is consisted of all three principal stresses. However, at fourth run a serious problem with obtaining convergence occurred, thus the mesh from the run three was used for the analyses. The locations, which were refined, are displayed in **Fig. 17**. Same mesh was used for analyses of the joints Type 1 and Type 2, but in the Type 2 a mesh of the reinforcement and different mesh of the bolt were added.

Table 3 Mesh sensitivity study.

Refinement #	Von Mises stress in the first ply	Element size	Mesh used for the analyses
1	32,9 MPa	1,3 mm	not used
2	36,5 MPa	1 mm	not used
3	41,2 MPa	0,3 mm	used
4	solution did not converge	0,2 mm	not used

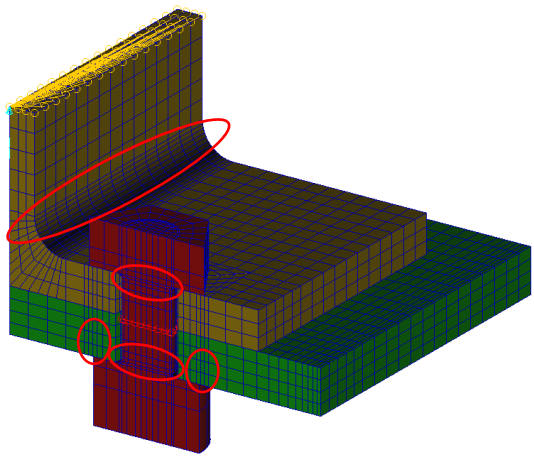

Fig. 17 Description of refined locations, refined locations in the red ellipses.

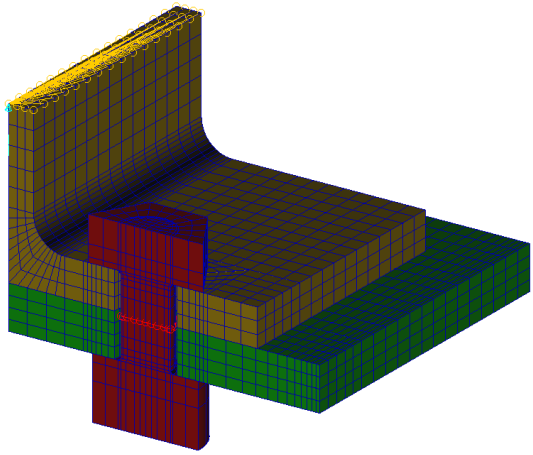

Fig. 18 Type 1 – meshed assembly.

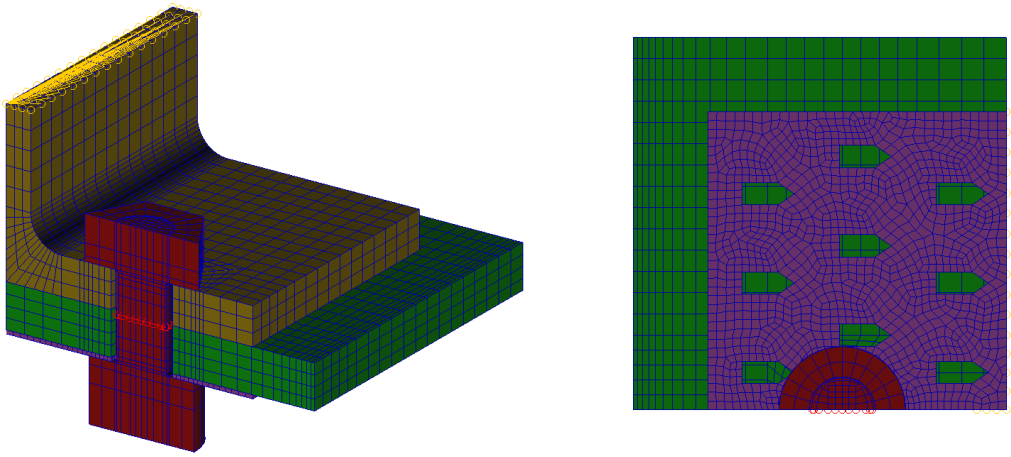

Fig. 19 Type 2 - meshed assembly, isometric view on the left, bottom view on the right.

7.3 Model of material

The laminated plate consists of 16 orthotropic plies, which mechanical properties are written in **Table 4**. and stacking sequence in **Table 5**. The plate cointains 4 elements through its thickness and each element has assigned *Laminate* property with the respective stacking sequence. The mesh with 4 element through thickness of the plate was chosen as a good balance between accuracy, computional time and stabililty of the solution. In Patran for describing a behaviour of composite two material models

were chosen: *Linear Elastic* and *Failure1 (SOL400/6000)* as shown in **Fig. 20**. Original material of the bracket was aluminium alloy D16, which is widely used for aircraft building.

Table 4 Material properties of one lamina of glass fiber reinforced polymer.

Property	**Symbol**	**Value**	**Unit**
Young's modulus	E_{11}	39 600	MPa
Young's modulus	E_{22}	20 600	MPa
Young's modulus	E_{33}	3 000	MPa
Poisson's s ratio	$\nu_{12} = \nu_{23} = \nu_{13}$	0,26	-
Shear modulus	$G_{12} = G_{23} = G_{13}$	5 100	MPa
Longitudinal tensile strength	F_{11t}	578	MPa
Transverse tensile strength	F_{22t}	385	MPa
Transverse tensile/compressive strength	$F_{33t} = F_{33c}$	26	MPa
Transverse compressive strength	F_{11c}	462	MPa
Transverse compressive strength	F_{22c}	321	MPa
Shear strength	F_{12}	45	MPa
Shear strength	$F_{23} = F_{13}$	22	MPa

Table 5 Stacking sequence.

Layer #	**Orientation (°)**	**Layer #**	**Orientation (°)**
1	0	**9**	90
2	45	**10**	-45
3	-45	**11**	45
4	0	**12**	90
5	90	**13**	0
6	45	**14**	-45
7	-45	**15**	45
8	90	**16**	0

Table 6 Material properties of aluminium alloy D16.

Property	Symbol	Value	Unit
Young's modulus	E	72 000	MPa
Poisson's ratio	ν	0,33	-
Yield point	σ_{yp}	351	MPa
Hardening slope	E_T	1600	MPa

Table 7 Materials properties for steel of the bolt.

Property	Symbol	Value	Unit
Young's modulus	E	207 000	MPa
Poisson's ratio	ν	0,3	-

Table 8 Material properties for steel of the reinforcement.

Property	Symbol	Value	Unit
Young's modulus	E	207 000	MPa
Poisson's ratio	ν	0,3	-
Yield point	σ_{yp}	500	MPa
Hardening slope	E_T	1600	MPa

7.3.1 Sensitivity study of residual stiffness factor

As the residual stiffness factor, which was described in detail in chapter **5.3**, is an important value for progressive failure analysis, the sensitivity study of the factor was done using various values of the factor and computational model of the joint Type 2. The results of the study are shown in **Fig. 21**. Similar study was done using the model Type 1. In the first case (Type 2), a problem with obtaining convergence occurred with values lower than 0,05 . In the case with the model Type 1 problems with obtaining convergence occurred with values lower than 0,15. As a good balance between accuracy and stabililty of solution, the value of residual stiffness factor 0,15 was chosen for both cases. According the study can be claimed the following statement:

"Too low values of residual stiffness factor can cause problems with achieving the convergence, too high values can make the model too stiff, thus inaccurate."

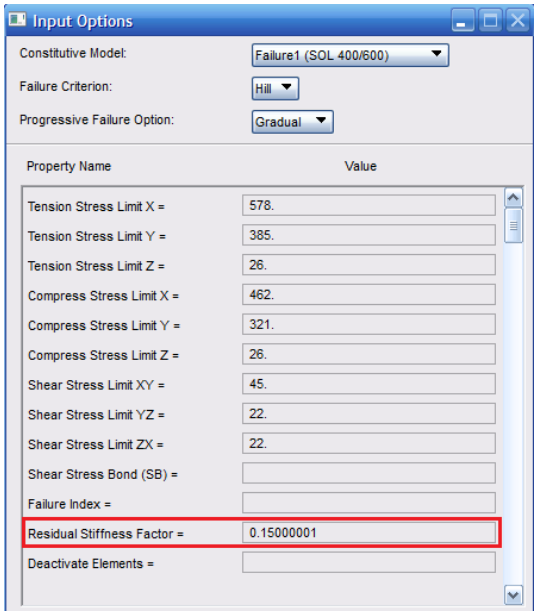

Fig. 20 Patran window for input strength limits, residual stiffness factor is in the red box.

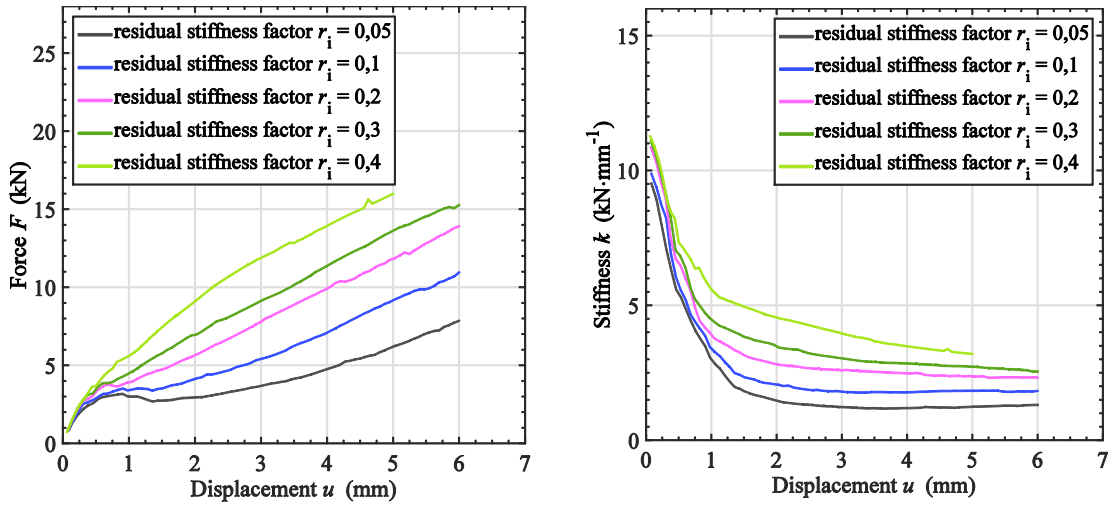

Fig. 21 Results of the sensitivity study of residual stiffness factor r_i using the computional model Type 2.

7.4 Model of boundary conditions

Due to symmetry two side surfaces of the whole assembly have assigned zero displacement in x-direction and in y-direction, and two side surfaces of the laminated plate were clamped. In adition, the model Type 2 has set symmetrical boundary conditions in x-direction and in y-direction on two surfaces of the reinforcement. All the boundary conditions are shown in **Fig. 22**.

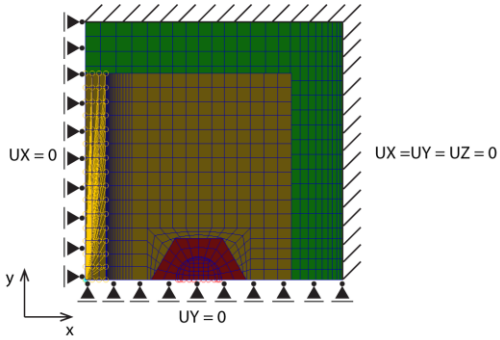

Fig. 22 Boundary conditions.

7.5 Contacts

Nastran Implicit Nonlinear uses the concept of contact bodies, thus contacts were set as shown in **Table 9** and **Table 10**. Nonlinear touched contacts were used in both cases with coefficient of friction $f = 0{,}61$, which was determined for friction between steel and aluminium according to Shigley [8]. Example of values of geometrical and physical properties, which were used in the analyses are shown in **Table 11** and **Table 12**. In both cases a problem was with a stabilization of the bolt inside the hole, thus achieving convergence, therefore the bolt was stabilized by four symmetrically located weak springs with stiffness 50 N·mm^{-1} as shown in **Fig. 25**.

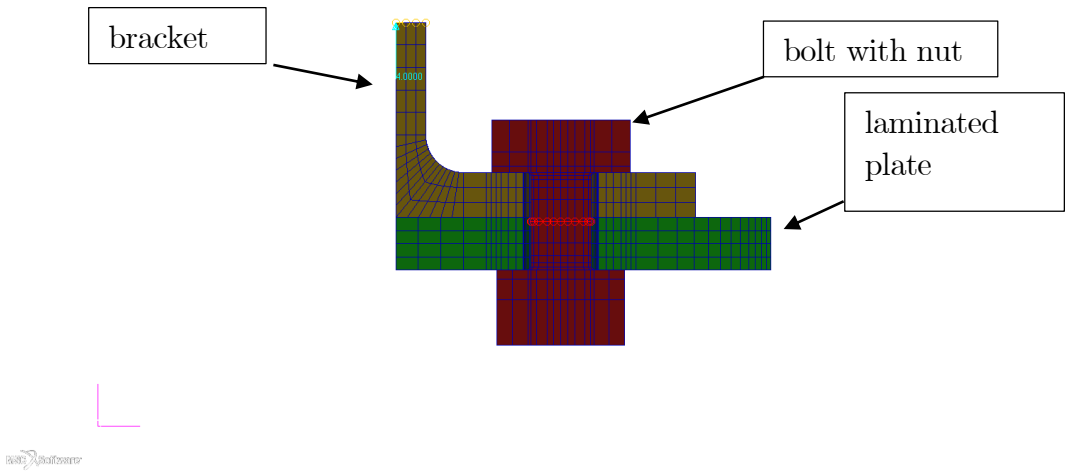

Fig. 23 Description of used contact bodies of Type 1.

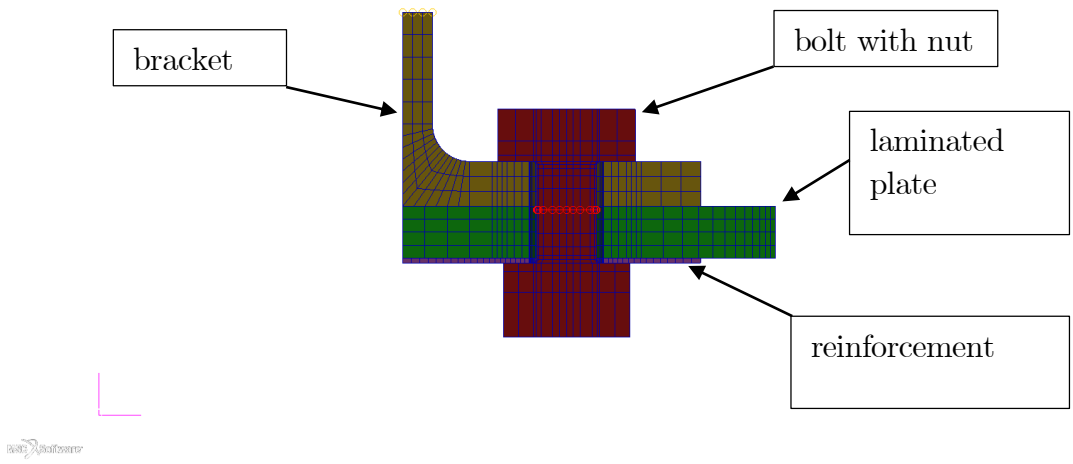

Fig. 24 Description of used contact bodies of Type 2.

Table 9 List of contact used in model Type 1

Contact pair	Type
bracket - bolt	touched
bracket - laminated plate	touched
laminated plate - bolt	touched

Table 10 List of contact used in model Type 2.

Contact pair	Type
bracket - bolt	touched
bracket - laminated plate	touched
laminated plate - bolt	touched
laminated plate - reinforcement	glued

Table 11 Geometrical properties of touched contact.

Property Name	Value
Distance Tolerance	-1
Bias Factor	0,9
Interference Closure	0
Side Off Distance	0
Hard-Soft Ratio	2

Glued Contact	No
Retain Gaps/Overlaps	No
Retain Moment/Overlaps	No

Table 12 Physical properties of touched contact.

Property Name	**Value**
Separation Threshold	0
Friction Coefficient	0,61
Fric Stress Limit	1E+20
Breaking Glue	No
Max Normal Stress	0
Max Normal Stress	0
Breaking Glue-1 Exp	2
Breaking Glue-2 Exp	2

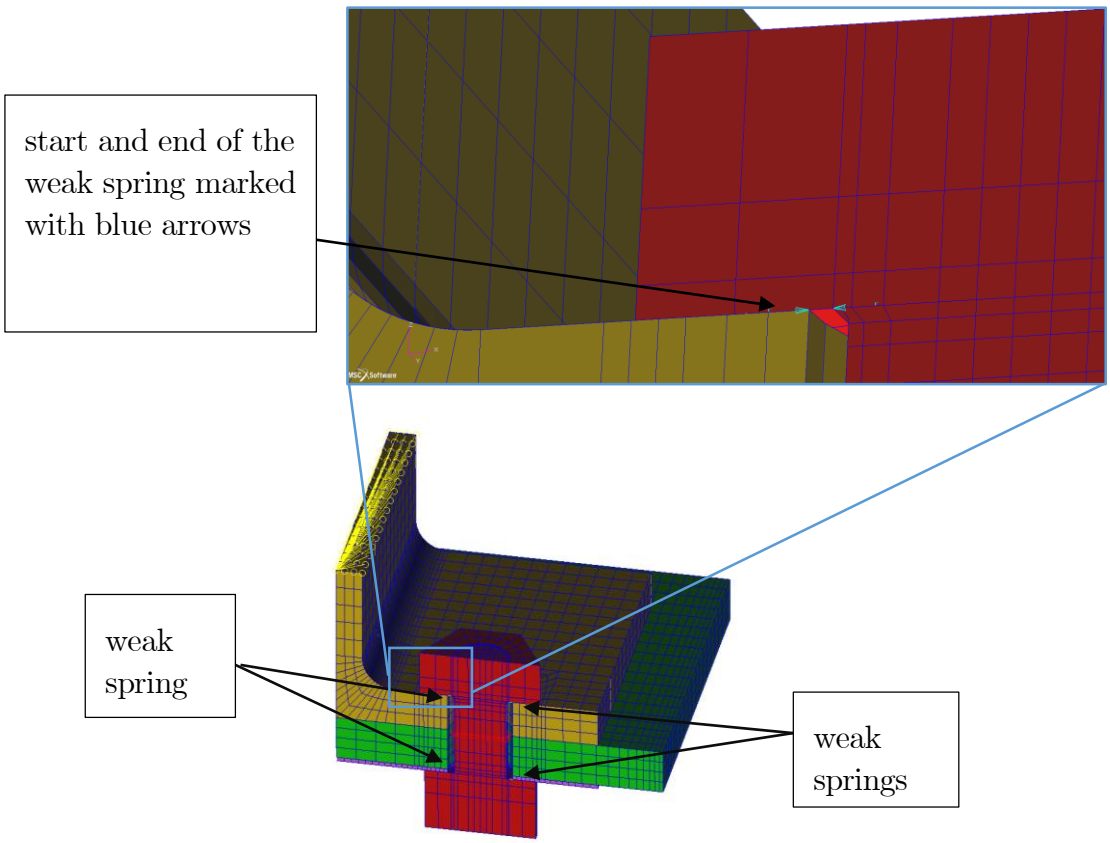

Fig. 25 Locations of weak spring for stabilization of the bolt inside the hole.

7.6 Model of loads

For transfer of load was in the location with coordinates (16.5, 0, 0) created a new node with number 1 and this node and the nodes on top of the T-part were coupled using Nastran RBE2 element as displayed in **Fig. 26**. The node number 1 is in the red circle.

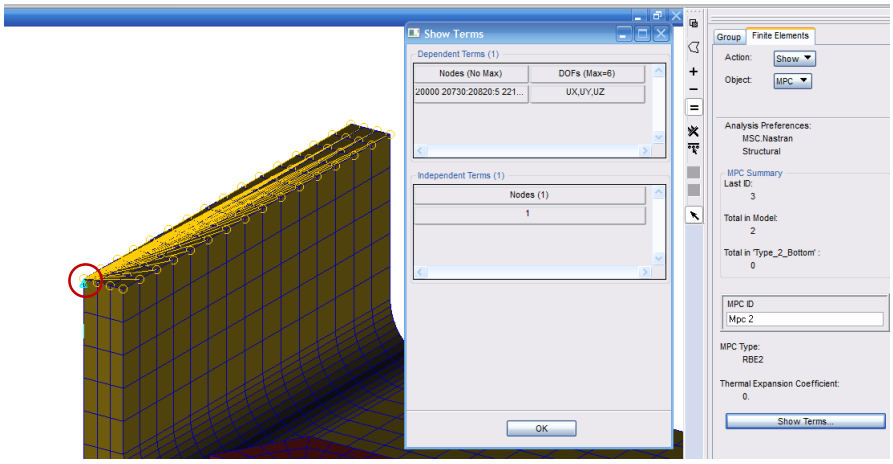

Fig. 26 Nastran RBE2 element.

As the nut of the bolt was turned with the torque 5,5 Nm, the preload had to be determined by the following equations according to Shigley [8], parameters of the bolt M5 was used according to Leinveber and Vávra [13].

$$M = K_{torque} F_{preload} d \tag{7.1}$$

$$H = 0{,}5 \cdot \sqrt{3} \cdot \ 0{,}8 = 0{,}69282 \text{ mm} \tag{7.2}$$

$$d_2 = d - \frac{3H}{4} = 5 - \frac{3 \cdot 0{,}69282}{4} = 4{,}48 \text{ mm} \tag{7.3}$$

$$\psi = \arctan \frac{P_h}{\pi d_2} = \arctan \frac{0{,}8}{\pi \cdot 4{,}48} = \text{ mm} \tag{7.4}$$

$$K_{torque} = \frac{d_2}{2d} \left[\frac{\tan \psi + f \sec(\alpha/2)}{1 - f\ (\tan \psi) \sec(\alpha/2)} \right] + 0{,}625 f_0 = 3{,}25325 \text{ mm}$$

$$= \frac{4{,}48}{2 \cdot 5} \left[\frac{\tan 3{,}25325 + 0{,}15 \cdot \sec(60/2)}{1 - 0{,}15 \cdot \tan 3{,}25325 \cdot \sec(60/2)} \right] + 0{,}625 \cdot 0{,}61 = 0{,}48534 \tag{7.5}$$

$$F_{preload} = \frac{M}{K_{torque} d} = \frac{5500}{0{,}48534 \cdot 5} = 2266 \text{ N} \tag{7.6}$$

where

M	(mm)	torque,
K_{torque}	(—)	coefficient of the torque,
d	(mm)	diameter of the thread,
d_2	(mm)	pitch diameter of the thread,
H	(mm)	height of the thread triangle
$F_{preload}$	(N)	preload,
f_0	(—)	coefficient of friction between nut and surface of the joined part, in this case friction occurs between steel and aluminium, thus according to [8] $f_0 = 0{,}61$
f	(—)	coefficient of friction between threads, according to [8] $f = 0{,}15$

The bolt preload was set as shown in **Fig. 27**. Since only one half of the bolt was modelled, the preload was halved as written in **Table 13**.

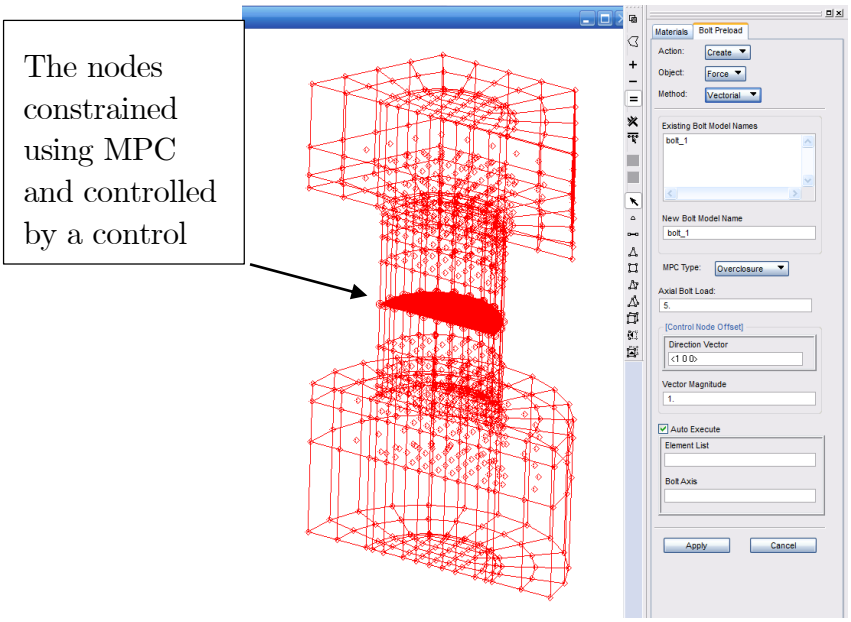

Fig. 27 Patran window for setting the bolt preload.

Table 13 The loads used in the analyses.

Number of the step	Load	Character	Location of applied load
Step 1	preload $P = 1133$ N	bolt pretension	Node 50 660
Step 2	displacement $u_z = 6$ mm	main load	Node 1

7.7 Setting of the solution

As nonlinear implicit solver was used, an apropriete settings of the solution is important. The values shown in **Fig. 28** were chosen according several trial runs in order to get accurate results, stable run and acceptable computional time. Large strains were set to on.

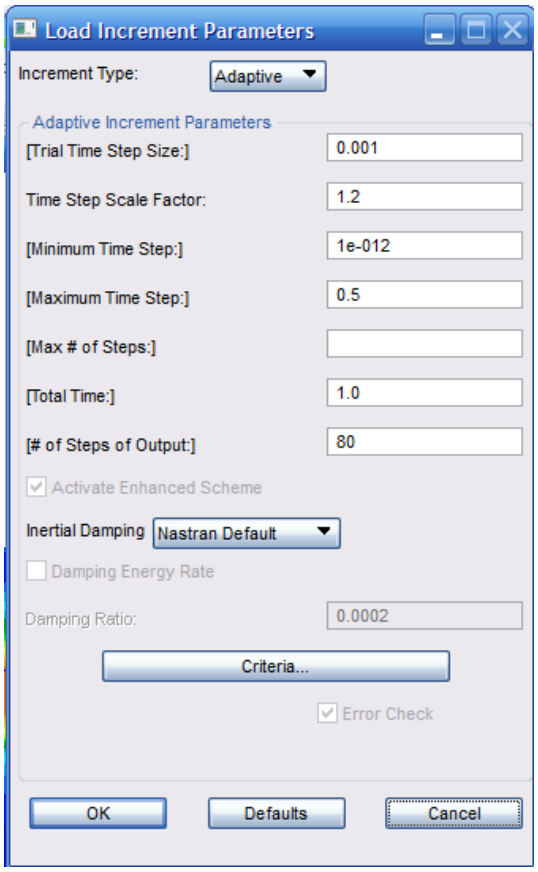

Fig. 28 Load increment parameters.

8 Results

Firstly, the force-displacement curves achieved by the experiment one average curve using arithmetic mean was determined for both joints as shown in **Fig. 29**. Force-displacement curves obtained from the FE analyses were saved from Patran to .xyd text file for further processing using Matlab. In Matlab force-displacement curves and stiffness-displacemenent curves were plotted, where stiffness k was determined using equation (8.1). Since only one-fourth models were built, the values of force were multiplied by four. Analyses of both models with Tsai-Wu criteria did not converge till the end, analysis with model Type 1 failed at displacement approximatelly 5 mm and analysis with model Type 2 stopped at displacement about 5,5 mm. Figures where are data from the analyses with Tsai-Wu criterion are marked with star *.

$$k = \frac{\mathrm{d}F}{\mathrm{d}u} \quad (\mathrm{kN} \cdot \mathrm{mm}^{-1}) \tag{8.1}$$

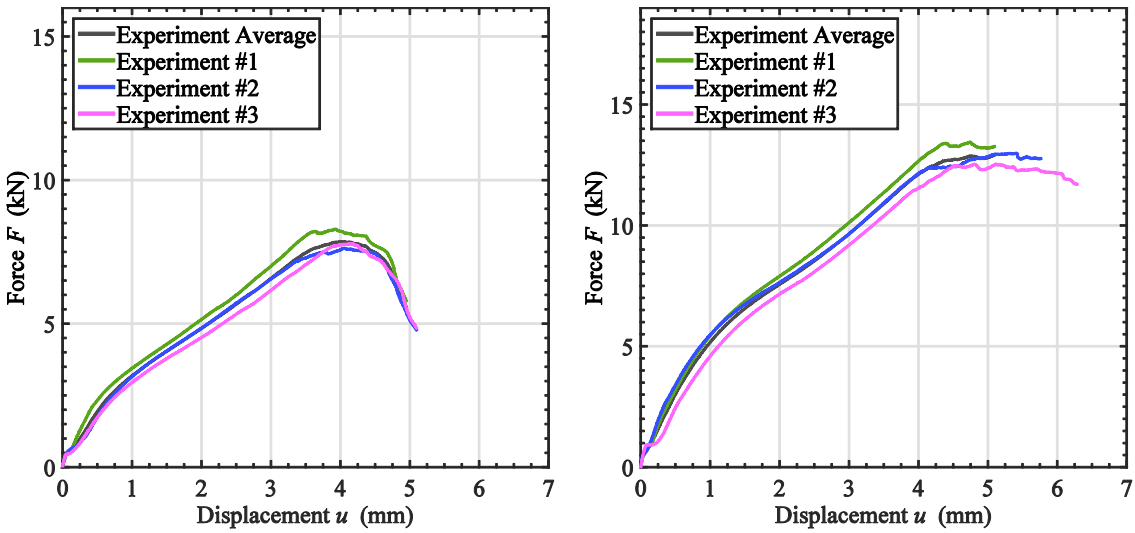

Fig. 29 Determination of average force-displacement curves from experimental data.

The bracket and bolt were designed so that the weakest part of whole assembly was the laminated plate, therefore the bolts or the bracket never failed during the experiments. This is the reason why the analyses were focused on the laminate, and bolt and bracket are not shown in the following figures.

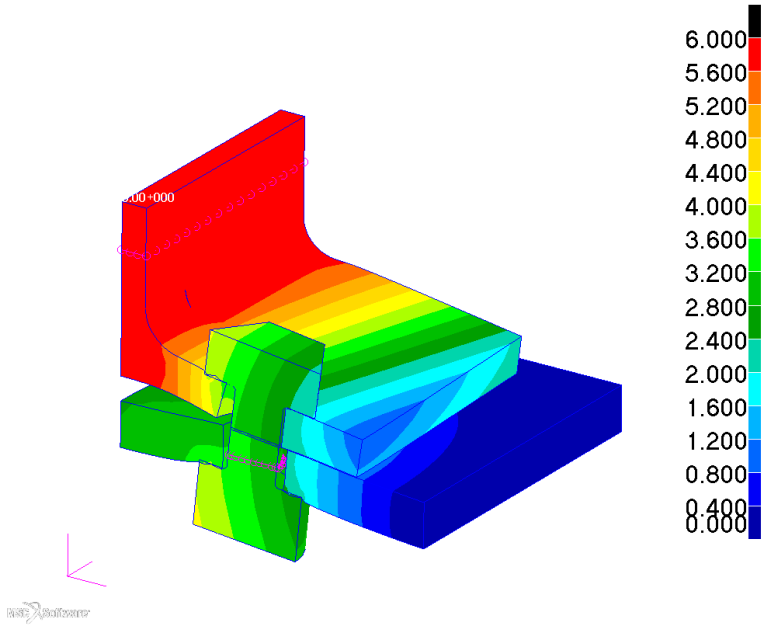

Fig. 30 Example of displacement of whole assembly of Type 1 with maximum stress criterion at the end of Step 2.

8.1 Type 1

8.1.1 Comparison of force-displacement curves and stiffness-displacement curves

In **Fig. 31** are plotted force-displacement and stiffness-displacement curves obtained by the FE analysis compared with experimental data. In general, the curves show not very good correlation.

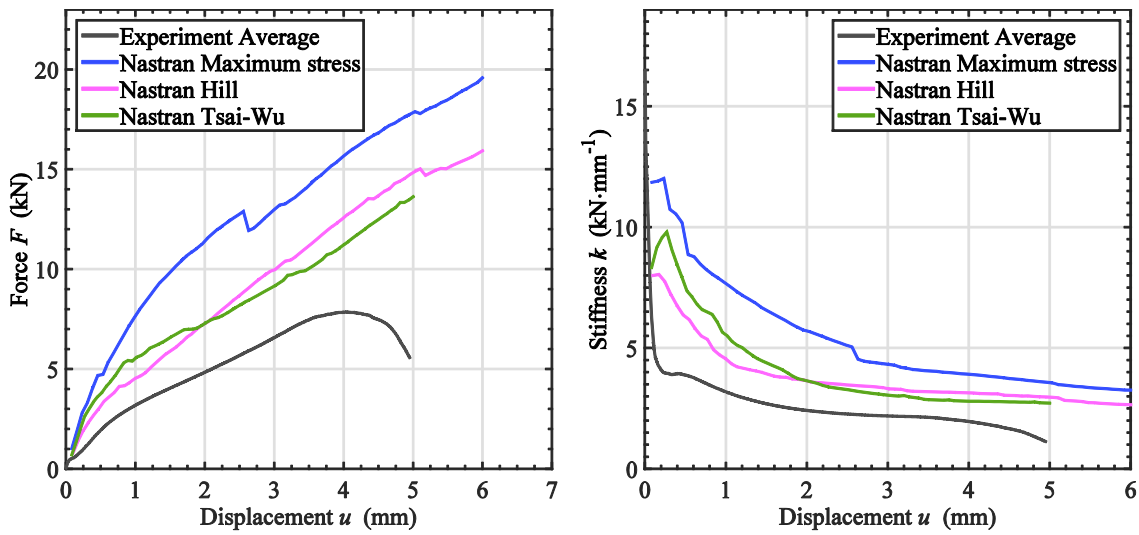

Fig. 31 Comparison of force-displacement curves and stiffness-displacement curves of Type 1 achieved by MSC Nastran and the experiment.*

8.1.2 Displacement and failure index using maximum stress failure criterion

In the following figures displacement and plots of failure index of Type 1 are shown at the end of Step 1 and at the end of Step 2 with maximum stress failure criterion, Hill failure criterion in chapter 8.1.3 and Tsai-Wu criterion in chapter 8.1.4. According to these figures, small local damage of the laminate occurs from the bolt preload.

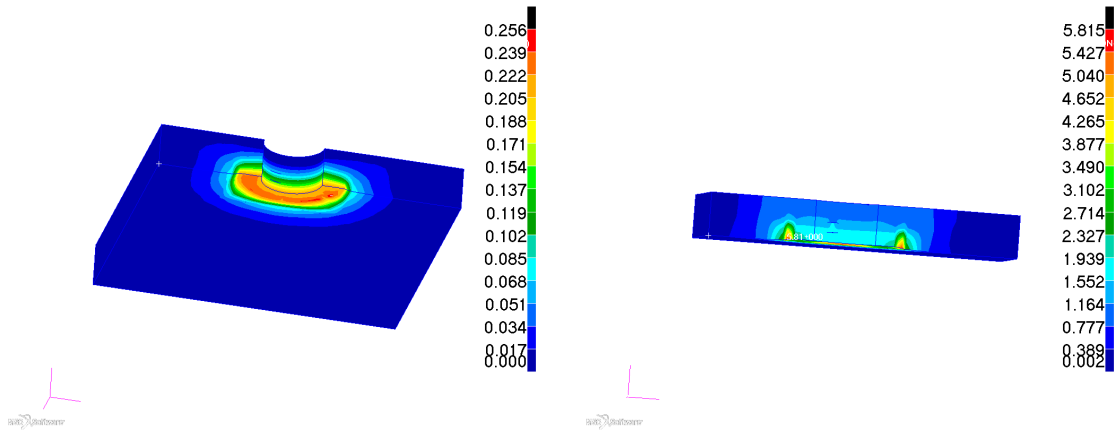

Fig. 32 Type 1 with maximum stress criterion. Results at the end of the Step 1: in the left image is displacement (mm) of the laminated plate in the left image, in the right image is shown failure index (-) for element.

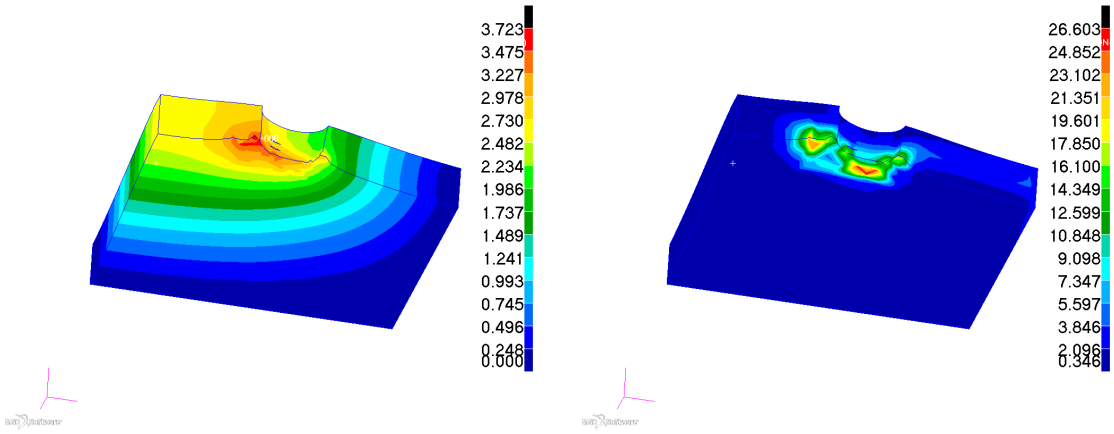

Fig. 33 Type 1 with maximum stress criterion. Results at the end of the Step 2: in the left image is displacement (mm) of the laminated plate in the left image, in the right image is shown failure index (-) for element.

8.1.3 Displacement and failure index using Hill failure criterion

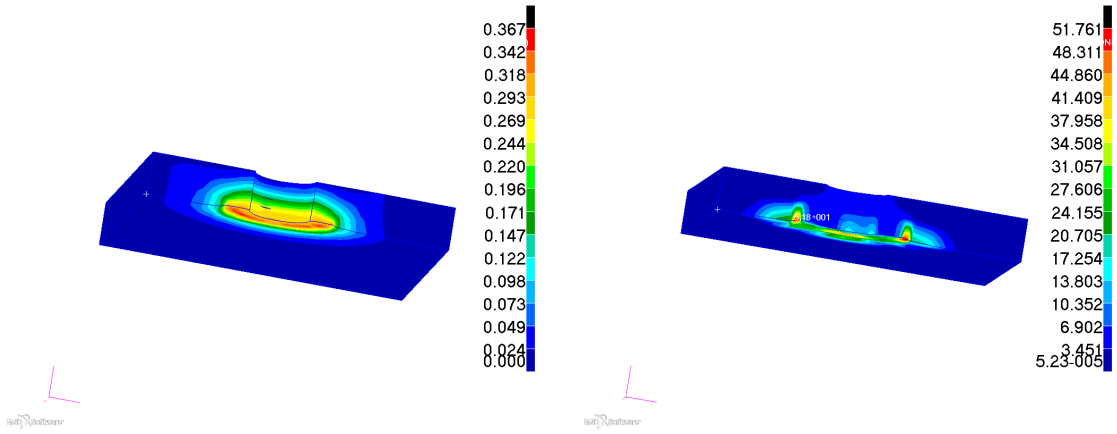

Fig. 34 Type 1 with Hill criterion. Results at the end of the Step 1: in the left image is displacement (mm) of the laminated plate in the left image, in the right image is shown failure index (-) for element.

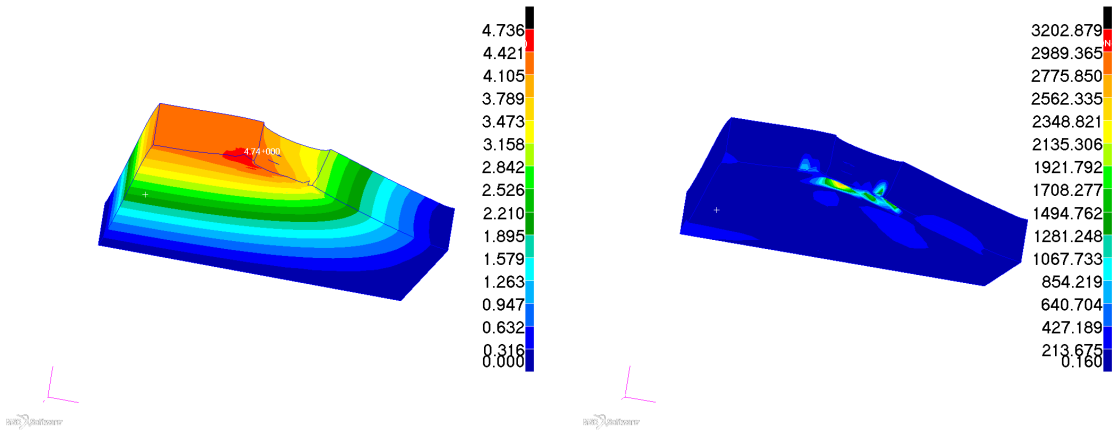

Fig. 35 Type 1 with Hill criterion. Results at the end of the Step 2: in the left image is displacement (mm) of the laminated plate in the left image, in the right image is shown failure index (-) for element.

8.1.4 Displacement and failure index using Tsai-Wu failure criterion*

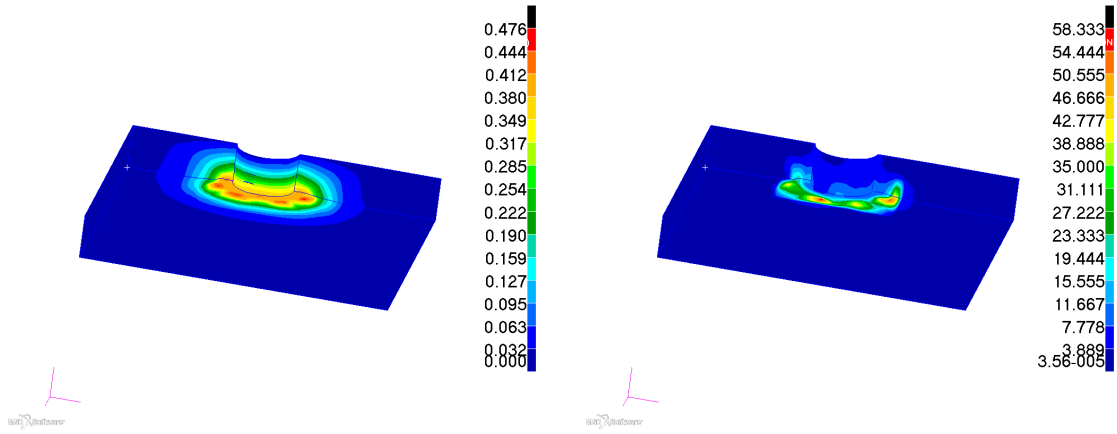

Fig. 36 Type 1 with Tsai-Wu criterion. Results at the end of the Step 1: in the left image is displacement (mm) of the laminated plate in the left image, in the right image is shown failure index (-) for element.

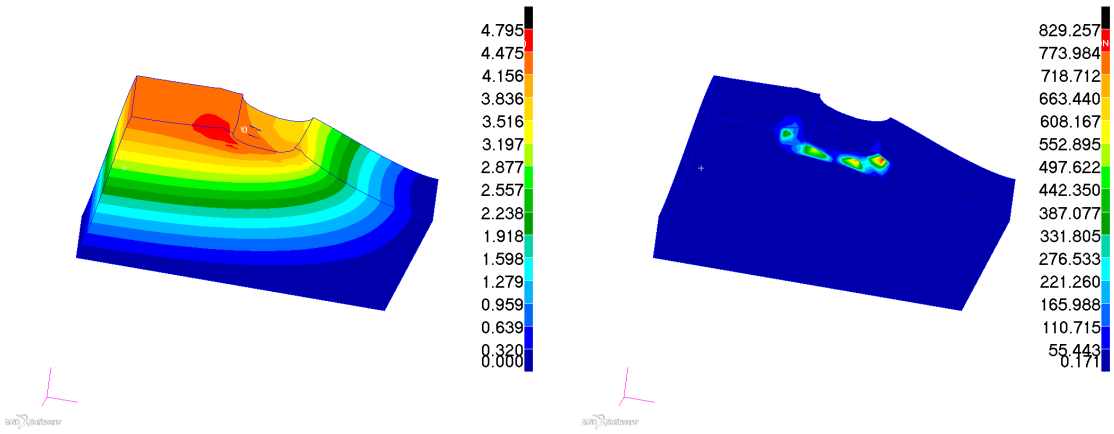

Fig. 37 Type 1 with Tsai-Wu criterion. Results at the end of the Step 2: in the left image is displacement (mm) of the laminated plate in the left image, in the right image is shown failure index (-) for element.*

8.2 Type 2

8.2.1 Comparison of force-displacement curves and stiffness-displacement curves

Unlike the comparison of the curves of Type 1 **Fig. 31**, the curves of Type 2 in **Fig. 38** display very good correlation in comparison with experimental data, especially with using Hill and Tsai-Wu failure criteria, even though the analysis with Tsai-Wu criteria failed due to a problem with achieving convergence.

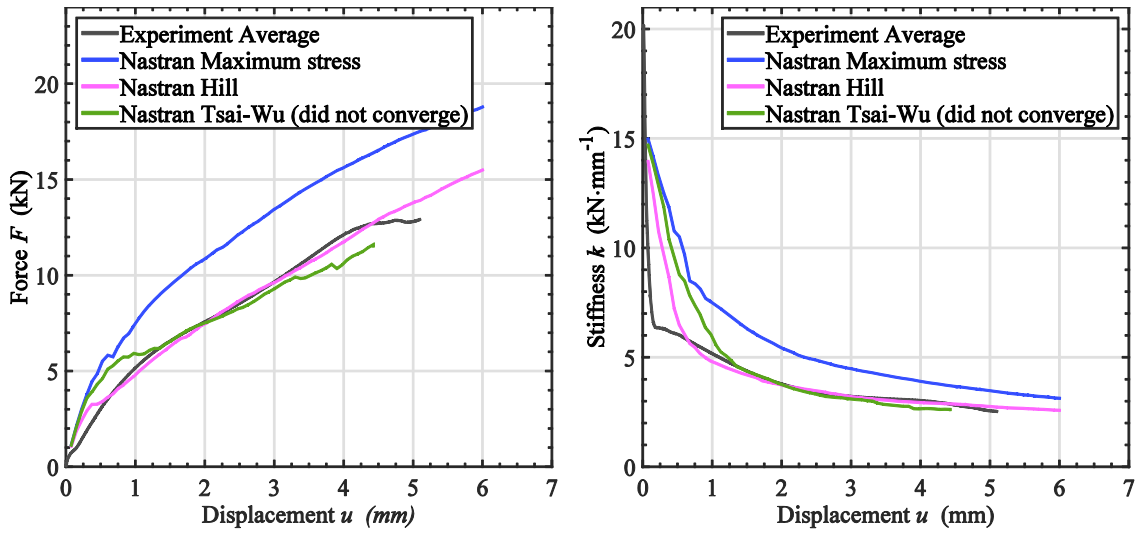

Fig. 38 Comparison of force-displacement curves and stiffnes-displacement curves of Type 2.*

8.2.2 Displacement and failure index using the maximum stress failure criterion

Similarly as for Type 1 in the previous figures, in the following figures displacement and plots of failure index of Type 2 are shown at the end of Step 1 and at the end of Step 2 with maximum stress failure criterion, Hill failure criterion in chapter 8.2.3 and Tsai-Wu criterion in chapter 8.2.4. According to the figures, small local damage of the laminate occured from the bolt preload.

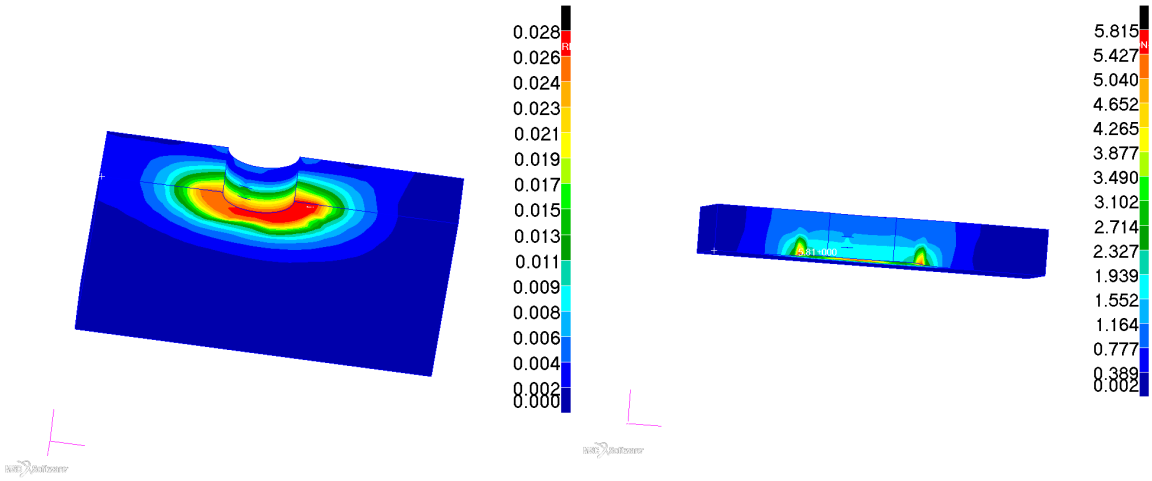

Fig. 39 Type 2 with maximum stress criterion. Results at the end of the Step 1: in the left image is displacement (mm) of the laminated plate in the left image, in the right image is shown failure index (-) for element.

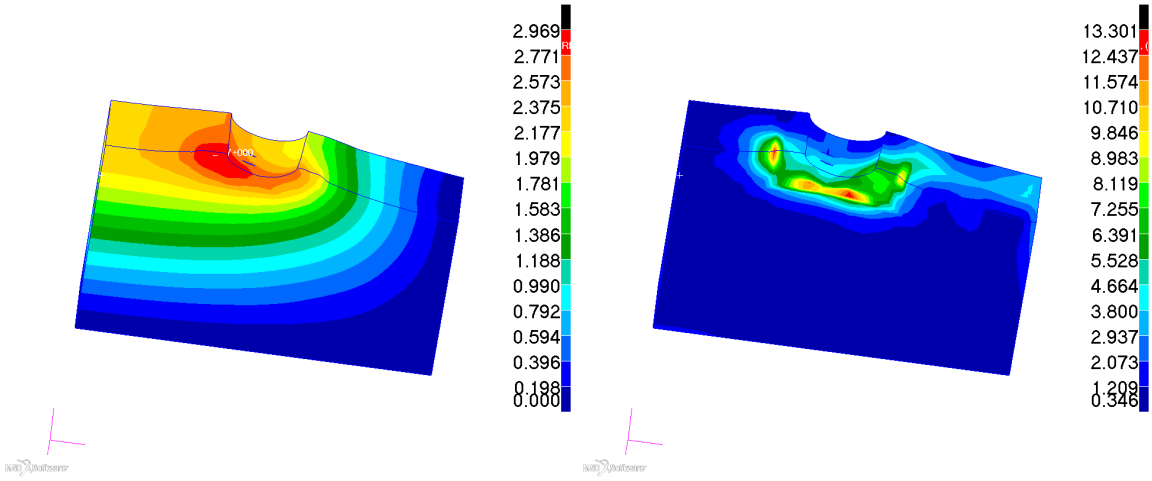

Fig. 40 Type 2 with maximum stress criterion. Results at the end of the Step 2: in the left image is displacement (mm) of the laminated plate in the left image, in the right image is shown failure index (-) for element.

8.2.3 Displacement and failure index using the Hill failure criterion

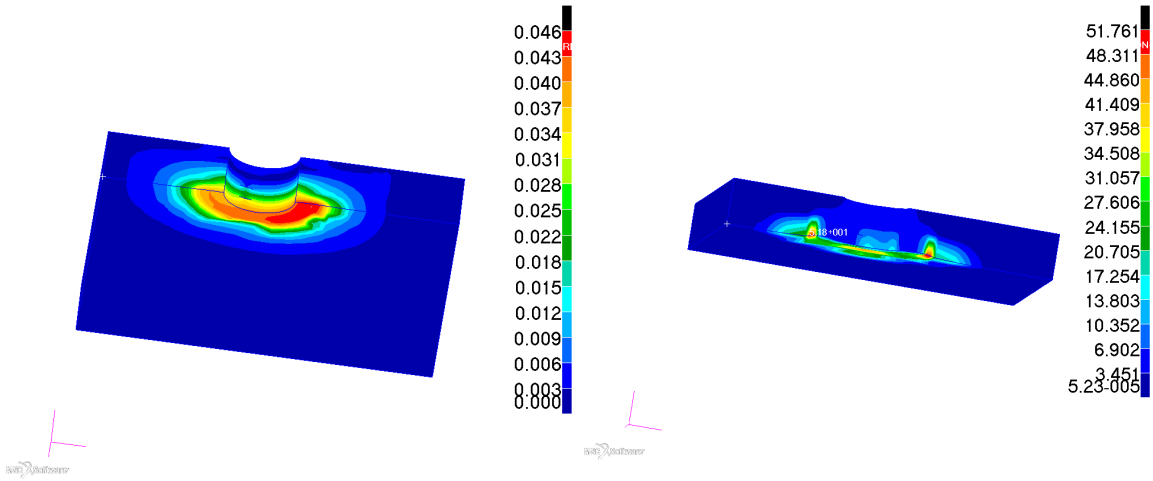

Fig. 41 Type 2 with Hill criterion. Results at the end of the Step 1: in the left image is displacement (mm) of the laminated plate in the left image, in the right image is shown failure index (-) for element.

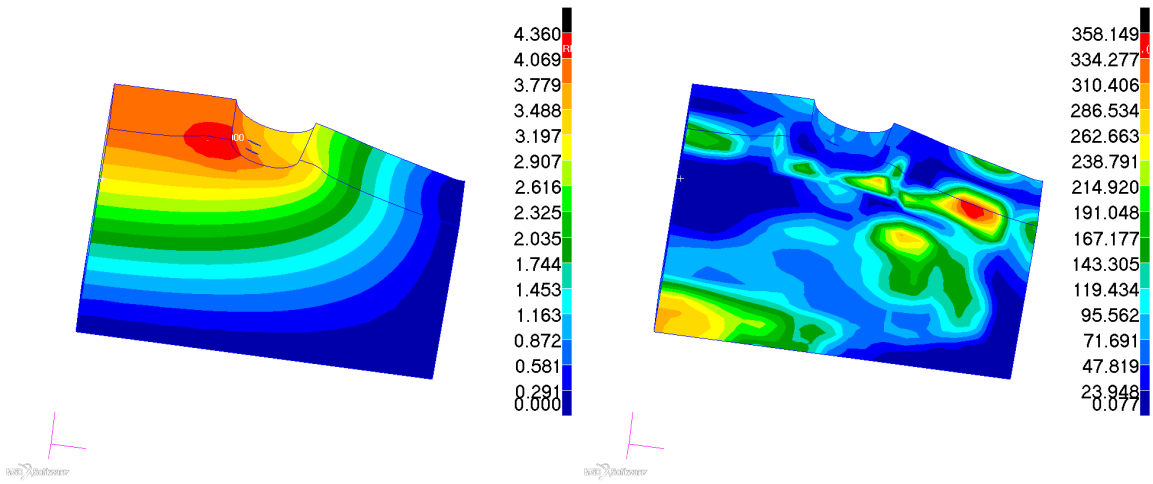

Fig. 42 Type 2 with Hill criterion. Results at the end of the Step 2: in the left image is displacement (mm) of the laminated plate in the left image, in the right image is shown failure index (-) for element.

8.2.4 Displacement and failure index using the Tsai-Wu failure criterion*

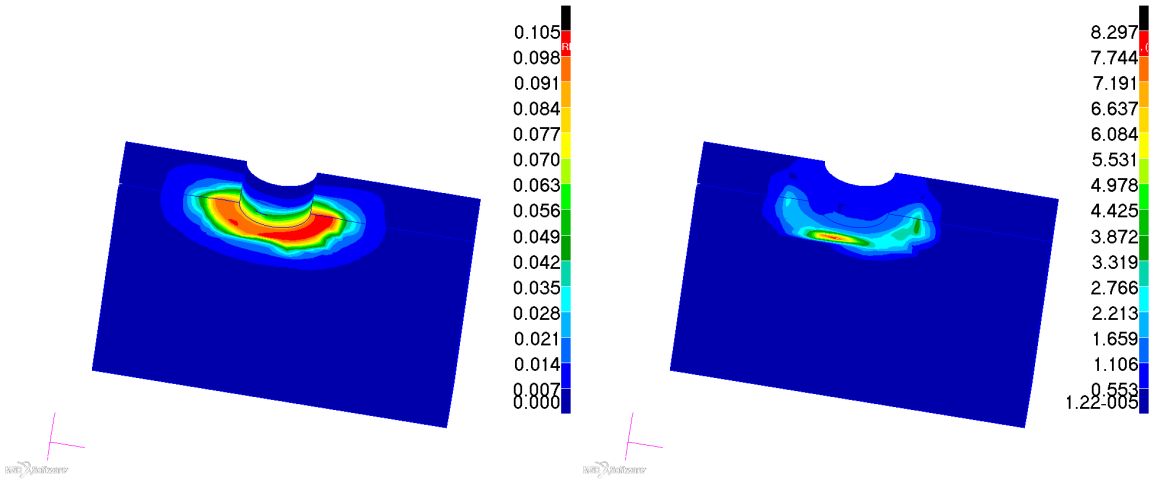

Fig. 43 Type 2 with Tsai-Wu criterion. Results at the end of the Step 1: in the left image translational displacements (mm) of the laminated plate are shown, in the right image failure index (-) for element is shown.

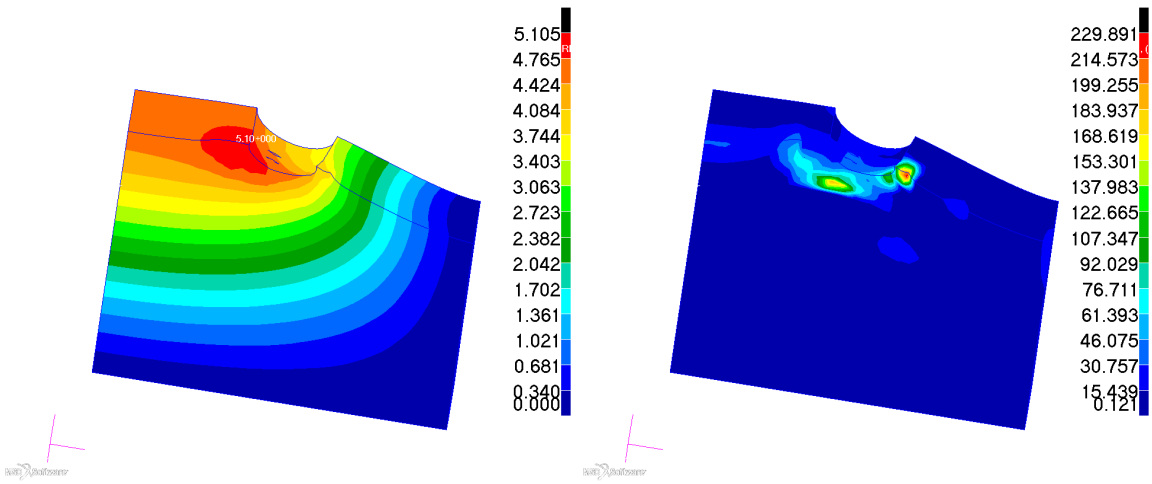

Fig. 44 Type 2 with Tsai-Wu criterion. Results at the end of the Step 2: in the left image is displacement (mm) of the laminated plate in the left image, in the right image is shown failure index (-) for element.*

8.3 Comparison of Type 1 and Type 2

The results of Type 1 and Type 2 were compared in the following graphs, **Fig. 45** describes comparison of force- displacement curves on the left and stiffness-displacement curves on the right obtained by experiments, where the clear difference in stiffnes can be seen in the right graph.

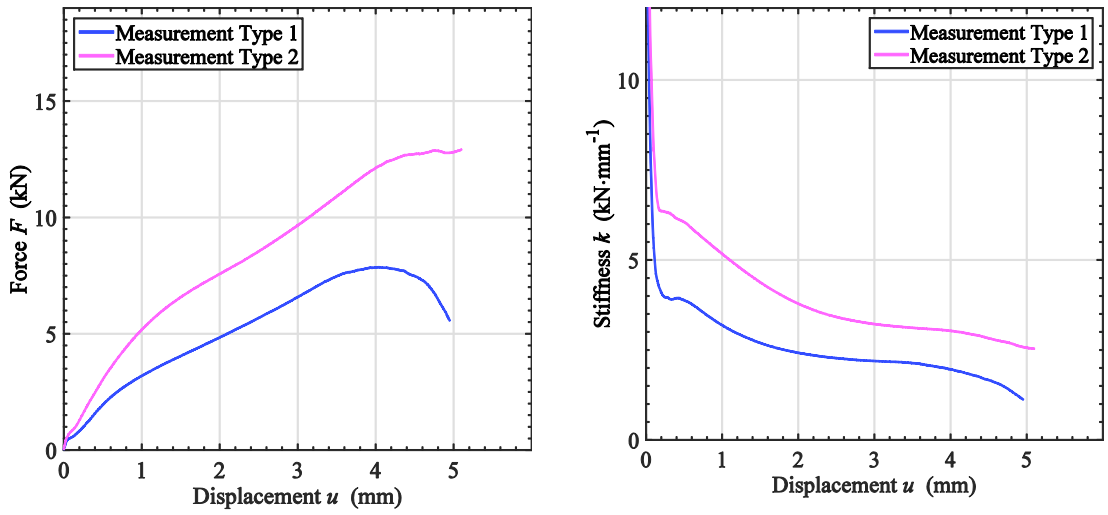

Fig. 45 Comparison of force-displacement curves on the left and stiffness-displacement curves on the right of Type 1 and Type 2 obtained by the measurement.

The curves got by FE analyses were compared too and they are displayed in the following graphs. These curves show quite good agreement, nevertheless, in these cases, a distinction between the curves should be much larger like it is shown in **Fig. 46**.

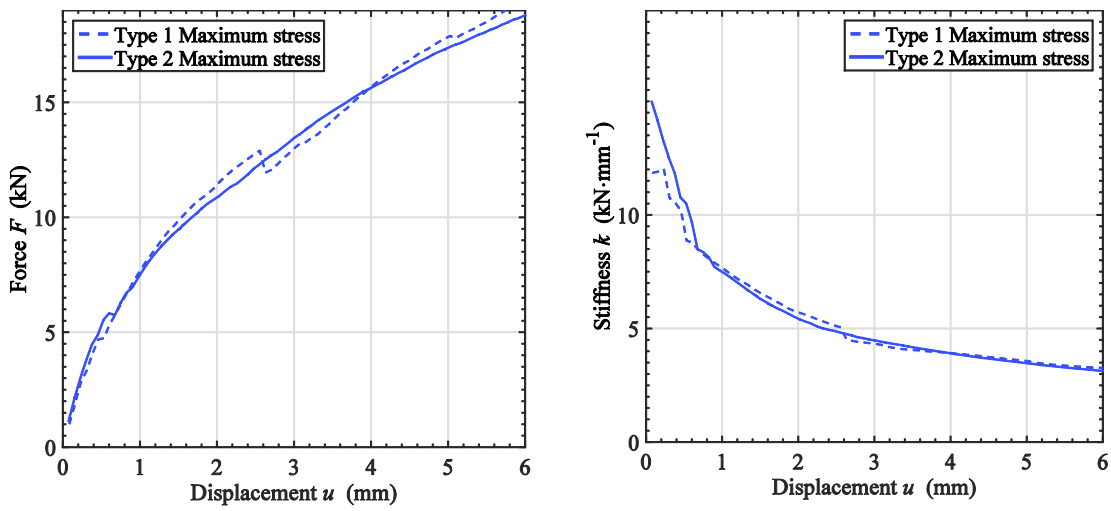

Fig. 46 Comparison of force-displacement curves on the left and stiffnes-displacement curves on the right of Type 1 an Type 2 obtained by FE analysis using maximum stress failure criterion.

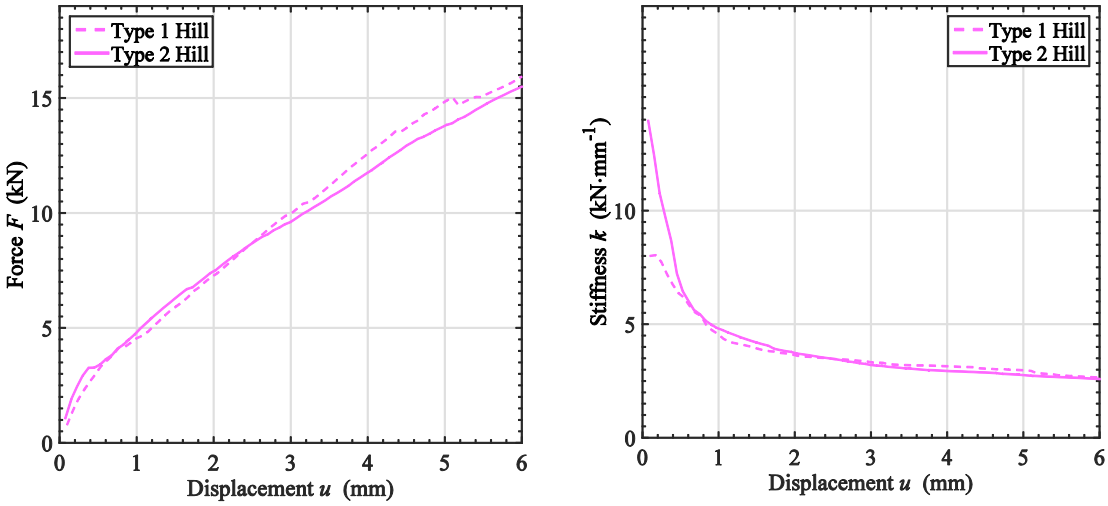

Fig. 47 Comparison of force-displacement curves on the left and stiffnes-displacement curves on the right of Type 1 an Type 2 obtained by FE analysis using Hill failure criterion.

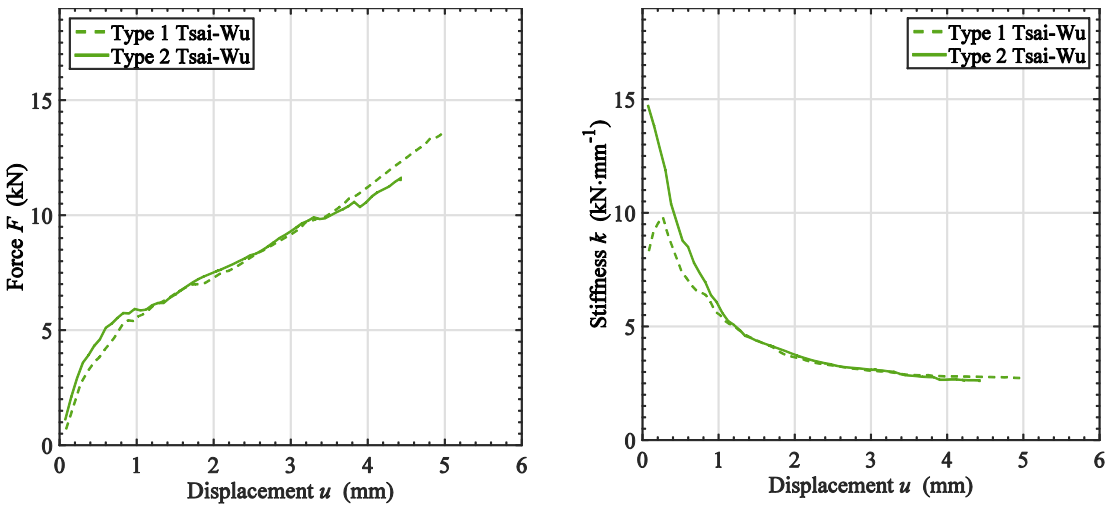

Fig. 48 Comparison of force-displacement curves on the left and stiffnes-displacement curves on the right of Type 1 an Type 2 obtained by FE analysis using Tsai-Wu failure criterion.*

8.3.1 Evaluation of loads at ultimate displacement

According to **Fig. 31** and **Fig. 38** the force-displacement curves do not have a global maximum as curves from experimental data do. One of the reasons can be too high values of the stiffness residual factor. However, if the values of the factor had been lower, no curves would be achieved due to the problem with convergence. This is the

reason why ultimate loads could not be obtained by Nastran solver. Nevertheless, values of ultimate load were obtained from experimental data, thus for evaluation of both models a different method was used — loads were compared at value of ultimate displacement. The procedure of evaluation of loads at ultimate displacement is written below:

1. determination of a displacement at the ultimate load from experimental data as shown in **Fig. 49** and plotting a vertical line at the value of the ultimate displacement in the previous step,
2. an intersection of the vertical line and force-displacement curve will determine a value of the load at the ultimate displacement as depicted in **Fig. 50**,
3. an comparison of the values of loads at the ultimate displacement as displayed in **Fig. 51**.

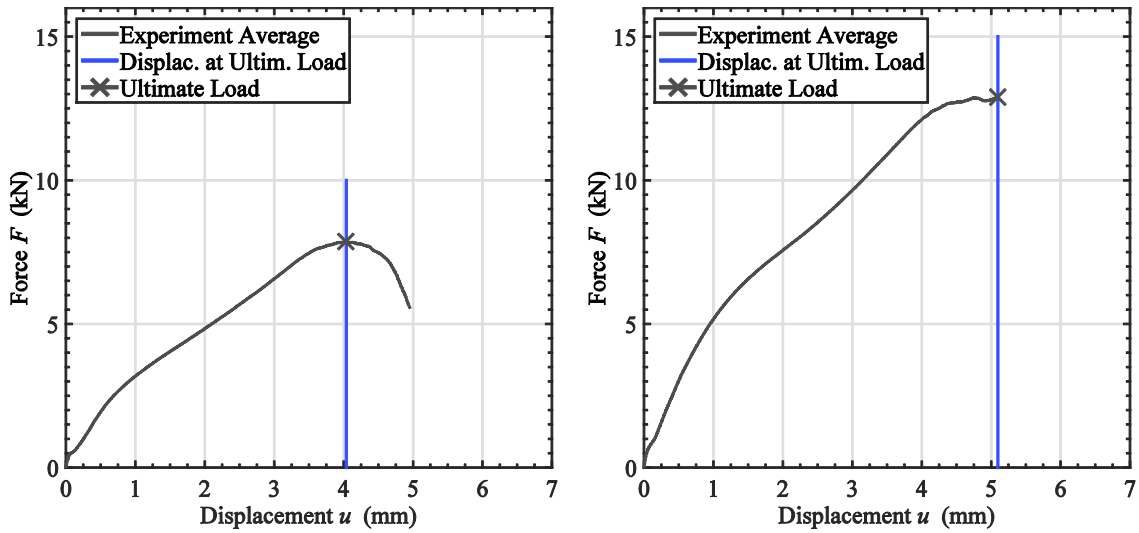

Fig. 49 Determination of the ultimate load and ultimate displacement of Type 1 on the left and Type 2 on the right using Matlab from experimental data.

The values of ultimate displacements and loads are written in the **Table 14**.

Table 14 The values of ultimate displacements and loads obtained by experiments.

Quantity	**Type 1**	**Type 2**
ultimate displacement (mm)	4	5,1
ultimate load (kN)	7,9	12,9

Values of load at ultimate displacement obtained by Matlab were compared and results are displayed in bar charts in **Fig. 51**. According to the right graph in **Fig. 50**,

force-displacement curve with Tsai-Wu criterion did not intersect the vertical line, hence the maximum value of the curve was used in the bar chart in **Fig. 51**.

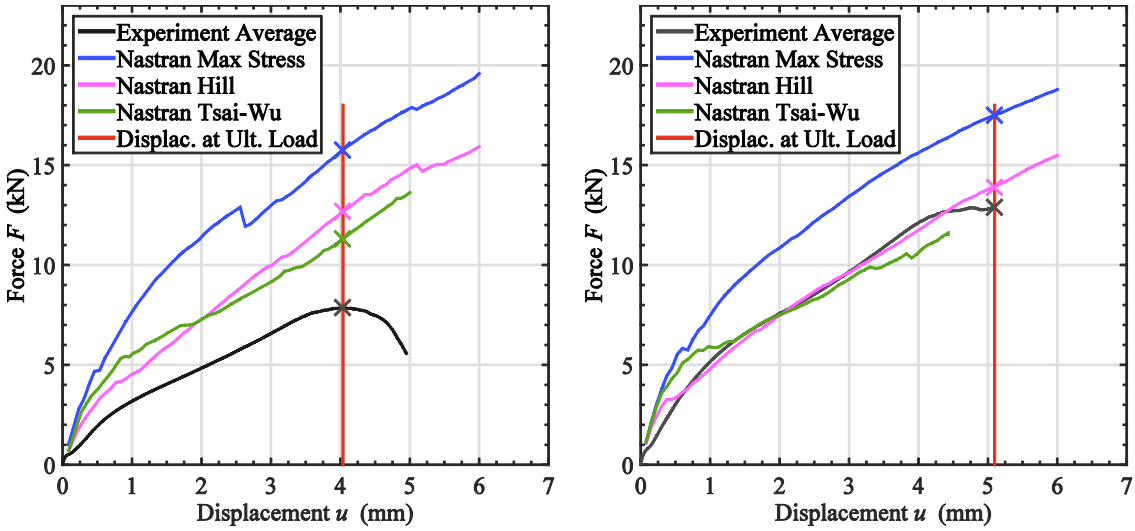

Fig. 50 Comparison of values of loads at ultimate displacement; Type 1 on the left, Type 2 on the right.*

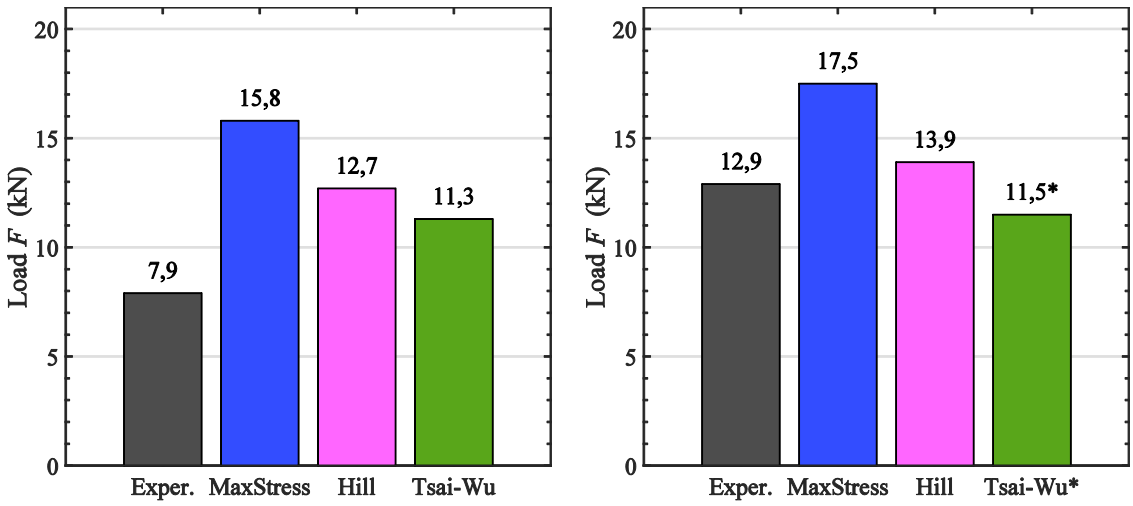

Fig. 51 Comparison of loads F at displacement $u_z = 4$ mm of Type 1 in the left graph; comparison of loads F at displacement $u_z = 5{,}1$ mm of Type 2 in the right graph.*

9 Discussion

For the progressive failure analyses was chosen Nastran implicit nonlinear solver, which has capability for description of post first-ply-failure of composites. Its main advantages against explicit solver is acceptable duration of analysis run and built-in several failure criteria, however known disadvantage of implicit solver is problem with convergence during solving highly nonlinear problems. Since explicit solver needs to set a time step, that must be less than the time which it takes a sound wave to travel across an element, an analysis with small elements lasts long. However, the situation is worse due to a need for use of damage material model for fiber composites, thus the unacceptable computation time was the reason why explicit solver could not be used as described in chapter 7.

The computational model of Type 1 was consisted of the laminate, the bolt with nut and the bracket. The model of the laminate was modelled with four elements through-thickness because higher values of elements led to sudden termination of run. The reason was high distortion of elements, and this caused the problem with convergence. The bolt was modelled with nut without threads, which do not affect overall stiffness. Same models of the laminate, the bracket and the bolt with nut were used for model Type 2. The reinforcement of the Type 2 was modelled without z-pins, which according to Mouritz [28] affect especially interlaminar mechanical properties, thus they were not modelled. Omitted entities and quantities were summarized in **Table 15**. In chapter 7.3.1 the sensitivity studies of residual stiffnes factor were done because the factor considerably affects results. For analyses was used the lowest value of the factor at which analysis run steadily.

In chapter 8 results of progressive failure analyses were placed. Stiffness of Type 1 in **Fig. 29** decreased generally lower than stiffness obtained from experimental data. The non-interactive criterion maximum stress gave the worst prediction of post FPF behavior compared to interactive criteria Hill and Tsai-Wu. Stiffness with Tsai-Wu criterion firstly rose rapidly and reached its highest point, then fell down gradually unlike stiffness with Hill criterion that just gradually declined.

Fig. 32 — **Fig. 37** describe displacement and failure indeces of Type 1 using three different failure criteria. Interesting fact is that in **Fig. 32**, **Fig. 36** and **Fig. 34** values of failure indeces are higher than one, that means a small local damage occurred at the end of Step 1 — which was caused by the bolt preload. Values of failure indeces in **Fig. 40**, **Fig. 42** and **Fig. 44** should be taken very carefully, because elements are in this state highly distorted, hence computed failure indeces do not show correct results.

Table 15 Summary of omitted entities and influences.

Name	Field	Justification
the thread	geometry	As the thread itself is not required for overall stiffness of the joints, it was not modelled.
the pins of the reinforcement	geometry	The pins are strongly connected to laminated plate and according to Mouritz [28] they affect especially interlaminar mechanical properties, which were not investigated in this work, thus z-pins were not modelled.
temperature	physical quatity	Temperature was constant during the measurement.
humidity	physical quantity	Humidity was constant during the measurement.
delamination	physical phenomenon	Interlaminar properties of laminate were not investigated in this work.

In the case of Type 2 in **Fig. 38** stiffness achieved by the experiment fell dramatically at the beginning than stiffness obtained using Nastran. Then, stiffness with Hill and Tsai-Wu criterion decreased sharply but not as stiffness from the experiment, at displacement 1,8 mm they reach same level as experimental data and decreased slightly till the end. The non-interactive criterion maximum stress gave again the worst prediction of post first-ply-failure behavior compared to interactive criteria Hill and Tsai-Wu.

Displacement and failure indeces of Type 1 using three different failure criteria are illustrated in **Fig. 32** — **Fig. 37**. The bolt preload caused small local damage also in the case of Type 2 as demonstrated in **Fig. 39**, **Fig. 41** and **Fig. 43**. Here again, the elements at the end of Step 2 are highly distorted, thus values of failure indeces in **Fig. 40**, **Fig. 42** and **Fig. 44** are not very correct, and therefore they should be considered very cautiously.

Comparison of results of Type 1 and 2 were placed in chapter 8.3 Comparison of Type 1 and Type 2. Firstly, force-displacement and stiffness-displacement curves were compared in **Fig. 45**. According to the right graph a difference in stiffness is approximately 2 $kN \cdot mm^{-1}$. However, the difference in stiffness using the finite element method with the non-interactive criterion illustrated in the right graph in **Fig. 46** is only small. Similarly, the difference is very small also with interactive criteria Hill and Tsai-Wu in **Fig. 47** and **Fig. 48**. One reason of this behavior can be chosen value of residual stiffness factor, nevertheless, as written in chapter 7.3.1, the value could not be lower.

According to the text in chapter 8.3.1, the force-displacement curves do not have a global maximum as curves from the experiment do, therefore ultimate loads were obtained only from experimental data and could not be compared with results of finite element analyses. However, loads at ultimate displacement were compared instead in **Fig. 50** and **Fig. 51**, where in respective graphs a difference between used failure criteria is nicely illustrated, which can help to choose a right criterion for evaluation of composite structure.

10 Conclusion

The main aim of this thesis was investigation of post first-ply-failure of metal-to-composite joints with emphasis on laminate using three different failure criteria by the finite element method. One non-interactive criterion the maximum stress and two interactive criteria Hill and Tsai-Wu were used for studying behavior of composite material in the work.

In the introductory part of the thesis were described the analyzed problems and the research study of progressive failure analysis of bolted joints, mechanics of composite materials and the finite element method. Computional models were depicted in the chapter 7, where important sensitivity studies of residual stiffness factor were described too and in the chapter 8 were placed results of the performed analyses.

According these results the following concluding statements can be claimed:

- In general, interactive criteria Hill and Tsai-Wu failure criteria gave similar prediction of post first-ply-failure behavior.
- Non-interactive criterion gave considerably higher values of force and stiffness than interactive criteria and its prediction of post first-ply-failure behavior is the worst compared to experimental data, thus interactive criteria are more apropriate for prediction of post FPF behavior of composites.
- Very good agreement of the results of FE analyses and the experiment had force-displacement curves of Type 2, especially with the Hill and Tsai-Wu criteria; the agreement in the case of the Type 1 is less satisfying. In general, the agreement is better in the case of Type 2 than in the case of Type 1.
- All the results are strongly dependant on the value of residual stiffness factor, thus accuracy can be increased, but too low values of the factor can result in problems with obtaining the convergence. Since the problems are caused mostly by extremely large distorsion of the elements, the solution of the problems can be a use of a different nonlinear solver, which allow the element death technique and remeshing. As Nastran Implicit Nonlinear SOL 400 does not allow such advanced methods, therefore these methods could not be used for the analyses. The most used solvers, which allow the element death technique and remeshing and have capability for the progressive failure analysis of composites, are MSC Marc and Abaqus. Explicit solver can be used too, but duration of analysis can take enormous time.
- If computional models are firstly harmonized according to experimental data, then the progressive failure analyses will give good prediction of post first-ply-failure behavior of material.

References

Books

[1] JANÍČEK, Přemysl. *Systémova metodologie: Brána do řešení problému.* 1st ed. Brno: CERM Academické vydavatelství, 2014. ISBN 978-80-7204-887-8.

[2] VRBKA, Jan. *Mechanika kompozitů.* In: *Insitute of solid mechanics, mechatronics and biomechanics FME BUT* [online], 2008. [cit. 2015-10-21] Available online on: https://www.vutbr.cz/www_base/priloha.php?dpid=83340

[3] DANIEL, Isaac. M. and Ori ISHAI. *Engineeering mechanics of composite materials.* 2nd ed. New York: Oxford University Press, 2006.ISBN 978-0-19-515097-1

[4] PETRUŠKA, Jindřich. *MKP v inženýrských výpočtech.* Brno university of technology FME: Institute of solid mechanics, mechatronics and biomechanics [online]. 2011. [cit. 2015-04-10]. Available online on: http://www.umt.fme.vutbr.cz/img/fckeditor/file/opory/RIV/MKP2011.pdf

[5] MALVERN, Lawrence E. *Introduction to the mechanics of a continuous medium.* New Jersey: Prentice-Hall, 1969. ISBN 978-0134876030

[6] JONES, Robert Millard. *Mechanics of composite materials.* 2nd ed. New York: Hemisphere Publishing Corporation, 1999. ISBN 1-56032-712-X

[7] BAKER, A., S. DUTTON and D. KELLY. *Composite Materials for Aircraft Structures.* 2nd ed. Reston: American Institute of Aeronautics and Astronautics , 2004. ISBN 1-56347-540-5

[8] SHIGLEY, J.E., C.R. MISCHKE and R.G BUDYNAS. *Kontruování strojních součástí.* Brno: VUTIUM Akademické vydavatelství, 2010. ISBN 978-80-214-2629-0

[9] JANÍČEK, P., J. MAREK a kol. *Expertní inženýrství v systémovém pojetí.* Praha: Grada Publishing, 2013. ISBN 978-80-247-4127-7

[10] ZIENKIEWICZ, Olgierd Cecil. *The finite element method. 5th ed., Volume 1: The Basis.* Oxford: Butterworth-Heinemann, 2000. ISBN 0-7506-5049-4

[11] LEINVEBER, Jan. and Pavel VÁVRA. *Strojnické tabulky.* 2nd ed. Úvaly: Albra, 2005. ISBN 80-7361-011-6

[12] NOVÁK, Kamil. *Analýza zbytkových napětí ve stěně tepny.* Brno, 2013. Master's thesis. Brno university of technology, Faculty of mechanical engineering, Institute of mechanics, mechatronics and biomechanics.

[13] MSC Software. *MSC Nastran 2014 Nonlinear User's Guide SOL 400:* MSC Software, ® 2014.

[14] MSC Software. *MSC Patran User's Guide:* MSC Software, ® 2014.

Scientific reasearch papers

[15] HART-SMITH, L. J. Design and empirical analysis of bolted or riveted joints. *Joining Fibre-Reinforced Plastics.* 1987, pp. 227-269.

[16] TSAI, Stephen W. A general theory of strength for anisotropic materials. *Journal of composite materials.* 1971, vol.5 : pp. 58-80. Available online on: http://www.dtic.mil/cgi-bin/GetTRDoc?AD=ADA306350

[17] ADAM, L., C. BOUVET, B. CASTANIÉ, A. DAIDIÉ and E. BONHOMME. Discrete ply model of circular pull-through test of fasteners in laminates. *Composite Structures.* 2012, vol. 94: pp. 3082-3091. Available online on: http://www.sciencedirect.com/science/article/pii/S0263822312002176

[18] HEIMBS, S., S. SCHMEER, J. BLAUROCK and S. STEEGER. Static and dynamic failure behaviour of bolted joints in carbon fibre composites. *Composites: Part A Applied Science and Manufacturing.* 2013, vol 47: pp. 91-101. Available online on: http://www.sciencedirect.com/science/article/pii/S1359835X12003697

[19] KABCHE, J.P., V. CACCESE, K.A. BERUBE and R. BRAGG. Experimental characterization of hybrid composite-to-metal bolted joints under flexural loading. *Composites Part B.* 2007, vol. 38: pp. 66-78. Available online on: http://www.sciencedirect.com/science/article/pii/S135983680600059X

[20] KELLY, Gordon and Stefan HALLSTROM. Strength and failure mechanisms of composite laminates subject to localised transverse loading. *Composite structures.* 2005, vol. 69: pp. 301-314. Available online on: http://www.sciencedirect.com/science/article/pii/S0263822304002375

[21] CATALANOTTI, G., P.P CAMANHO, P. GHYS and A.T MARQUES. Experimental and numerical study of fastener pull-through failure in GFRP laminates. *Composite structures.* 2011, vol. 94: pp. 239-245. Available online on: http://www.sciencedirect.com/science/article/pii/S0263822311002418

[22] ELDER, D.J., A.H. VERDAASDONK and R.S THOMSON. Fastener pull-through in a carbon fibre epoxy composite joint. *Composite structures.* 2008, vol. 86: pp. 291-298. Available online on: http://www.sciencedirect.com/science/article/pii/S0263822308000925

[23] STOCCHI, C., P. ROBINSON and S.T PINHO. A detailed finite element investigation of composite bolted joints with countersunk fasteners. *Composites Part A: Applied Science and Manufacturing.* 2013, vol. 52: pp. 143-150. Available online on: http://www.sciencedirect.com/science/article/pii/S1359835X1200303X

[24] CAMANHO, Pedro P. and F.L. MATTHEWS. Stress analysis and strength prediction of mechanically fastened joints in FRP. *Composite part A: Applied Science and manufacturing.* 1997, vol. 28: pp. 529-547. Available online on: http://www.sciencedirect.com/science/article/pii/S1359835X97000043

[25] MCCARTHY, C. T., M.A. MCCARTHY and V.P. LAWLOR. Progressive damage analysis of multi-bolt composite joints with variable bolt-hole clearance. *Composites Part B Engineering.* 2005, vol. 36: pp. 290-305. Available online on: http://www.sciencedirect.com/science/article/pii/S1359836804001404

[26] WANG, Z., S. ZHOU, J. ZHANG and L. ZHOU. Progressive failure analysis of bolted single-lap composite joint based on extended finite element method. *Materials & Design.* 2011, vol. 37: pp. 582-588. Available online on: http://www.sciencedirect.com/science/article/pii/S0261306911006054

[27] HÜHNE, C., A. K. ZERBST, G. KUHLMAN and R. ROLFES. Progressive damage analysis of composite bolted joints with liquid shim layers usint constant and continuous degradation models. *Composite Structures.* 2010, vol. 92: pp. 189-200. Available online on: http://www.sciencedirect.com/science/article/pii/S0263822309002049

[28] MOURITZ, Adrian P. Review of z-pinned composite laminates. *Composites: Part A.* 2007, vol. 38: pp. 2383-2397. Available online on: http://www.sciencedirect.com/science/article/pii/S1359835X07001479

Internet sources

[29] BURŠA, Jiří. *Constitutive relations of materials (lectures 2015).* In: *Institute of solid mechanics, mechatronics and biomechanics FME BUT* [online], 2015. [cit. 2015-11-18] Available online on: http://www.umt.fme.vutbr.cz/~jbursa/Konstitutivni%20modely.7z

[30] PETRUŠKA, Jindřich. *Nonlinear problems of mechanics in FEM.* In: *Institute of solid mechanics, mechatronics and biomechanics FME BUT* [online], 2015. [cit. 2015-04-11] Available online on: http://www.umt-old.fme.vutbr.cz/%7Ejpetruska/nelinearni_mechanika/RNK.zip

[31] MSC Software. *Composites Technology Day - Section 1 Introduction to Composites:* MSC Software, ® 2012. [online] [cit. 2016-03-05] Available online on: http://pages.mscsoftware.com/rs/mscsoftware/images/sec1_intro_to_composites_021712.pdf

[32] FLUGKERI2: *A350XWB-Demo.jpg.* In: https://commons.wikimedia.org/wiki [online]. 22 July 2015 [cit. 2016-01–02]. Available on: https://upload.wikimedia.org/wikipedia/commons/b/b1/A350XWB-Demo.jpg

List of symbols

Symbol	Unit	Quantity
d	mm	diameter of the thread
d_2	mm	pitch diameter of the thread
e	-	Euler's number, mathematical constant
E_{11}, E_{22}, E_{33}	MPa	Young's moduli
Eij^A	-	component of Almansi-Hamel strain tensor
Eij^C	-	component of logarithmic strain tensor
Eij^L	-	component of Green-Lagrange strain tensor
$\boldsymbol{F}$	N	global force matrix
f	-	coefficient of friction between threads
F	N	force
f_0	-	coefficient of friction between nut and surface of the joined part, in this case friction occurs between steel and aluminium
F_{11c}, F_{22c}, F_{33c}	MPa	compressive strength in respective directions
F_{11t}, F_{22t}, F_{33t}	MPa	tensile strengths in respective directions
F_{12}, F_{23}, F_{31}	MPa	shear strengths in respective directions
F_{index}	-	failure index
$F_{preload}$	N	bolt preload
G_{12}, G_{23}, G_{31}	MPa	shear moduli in respective directions
H	mm	height of the thread triangle
k	$kN\cdot mm^{-1}$	stiffness
$\boldsymbol{K}$	$N\cdot m^{-1}$	global stiffness matrix
$\boldsymbol{K}_{\mathrm{Ti}}$	$N\cdot m^{-1}$	tangent global stiffness matrix
K_{torque}	-	coefficient of the torque
M	Nmm	torque
$\boldsymbol{o}^T$	$N\cdot m^{-3}$	transpose distributed body forces matrix
$\boldsymbol{P}$	N	external load matrix
$\boldsymbol{p}^T$	Pa	transpose surface forces matrix
$\boldsymbol{R_i}$	N	residual forces matrix
r_i	-	residual stiffness factor
S_i	-	second Piola-Kirchhoff stress tensor

$\boldsymbol{U}$	m	global displacement matrix
$\boldsymbol{u_i}$	m	displacement matrix
$\boldsymbol{U}^T$	m	transpose displacement matrix
$\boldsymbol{u^T}$	m	transpose displacement matrix
u_z	mm	displacement in direction z
W	J	strain energy
X_1, X_2, X_3	m	coordinates of the particle in the Lagrangian description
x_1, x_2, x_3	m	coordinates of the particle in the Eulerian descrition
δ_F, δ_u		convergence criteria
$\boldsymbol{\Delta u_i}$	m	displacement increment
$\boldsymbol{\varepsilon}^T$	-	transpose strain matrix
λ_i	-	stretch ratio
ν_{12}, ν_{23}, ν_{31}	-	Poisson's ratios in respective directions
Π	J	total potential energy
$\boldsymbol{\pi}$	-	mathematical constant
σ_i	Pa	component of the first Piola-Kirchhoff stress tensor
$\boldsymbol{\sigma}^T$	Pa	transpose stress matrix
σ_{yp}	Pa	yield point, yield stress
$\boldsymbol{\tau}_i$	Pa	component of Cauchy stress tensor

List of abreviations and names of software

FEM	finite element method
PFA	progressive failure analysis
FPF	first-ply-failure
CFRP	carbon fiber reinforced polymer
GFRP	glass fiber reinforced polymer
MSC Marc	implicit nonlinear finite element solver
Abaqus	implicit and explicit nonlinear finite element solver
Ansys	implicit nonlinear finite element solver
MSC Nastran SOL 400	implicit nonlinear finite element solver
MSC Patran	preprocessor and postprocessor for preparation finite element models and evaluating results

List of figures

Fig. 1 Airbus A350XWB has fuselage and wings made of CFRP. [32] 12

Fig. 2 Schematics of the system of important quantities.[12] 15

Fig. 3 Technical drawing of the joint Type 1. 16

Fig. 4 Technical drawing of the joint Type 2. 17

Fig. 5 Schematic illustration of main failure modes in mechanical joints in composites.[15] 17

Fig. 6 Top side of laminated plates of the joints after the measurement; on the left Type 1, on the right Type 2. Published with permission of Institute of aerospace engineering of Brno university of technology. 18

Fig. 7 Bottom side of laminated plates of the joints after the measurement; on the left Type 1, on the right Type 2. Published with permission of Institute of aerospace engineering of Brno university of technology. 18

Fig. 8 Comparison of behaviour of isotropic, orthotropic and anisotropic material. [6] 21

Fig. 9 The base othotropic cooordinate system.[2] 22

Fig. 10 Loaded element of orthotropic material in principal orthotropic directions. [2] 23

Fig. 11 Failure envelope for unidirectional lamina under biaxial normal loading (maximum stress theory). [3] 24

Fig. 12 Failure envelopes for unidirectional E-glass/epoxy lamina under biaxial loading with different levels of shear stress (Tsai-Wu criterion). [3] 27

Fig. 13 Graphical representation of Newton-Raphson iterative solution. [30] 32

Fig. 14 Technical drawing of the joint Type1 clamped using the clamps for measurement, with red dashed lines demarked one fourth of joint, which was used for the computional models; same claping systém was used for testing the joint Type 2. 36

Fig. 15 Geometry of the computional model Type 1. 37

Fig. 16 Geometry of the computional model Type 2. 37

Fig. 17 Description of refined locations, refined locations in the red ellipses. 38

Fig. 18 Type 1 – meshed assembly. 39

Fig. 19 Type 2 - meshed assembly, isometric view on the left, bottom view on the right. .. 39

Fig. 20 Patran window for input strength limits, residual stiffness factor is in the red box. 42

Fig. 21 Results of the sensitivity study of residual stiffness factor r_1 using the computional model Type 2. 42

Fig. 22 Boundary conditions. 43

Fig. 23 Description of used contact bodies of Type 1. 43

Fig. 24 Description of used contact bodies of Type 2. 44

Fig. 25 Locations of weak spring for stabilization of the bolt inside the hole. 45

Fig. 26 Nastran RBE2 element. 46

Fig. 27 Patran window for setting the bolt preload. 47

Fig. 28 Load increment parameters. 48

Fig. 29 Determination of average force-displacement curves from experimental data. 49

Fig. 30 Example of displacement of whole assembly of Type 1 with maximum stress criterion at the end of Step 2. 50

Fig. 31 Comparison of force-displacement curves and stiffness-displacement curves of Type 1 achieved by MSC Nastran and the experiment.* 50

Fig. 32 Type 1 with maximum stress criterion. Results at the end of the Step 1: in the left image is displacement (mm) of the laminated plate in the left image, in the right image is shown failure index (-) for element. 51

Fig. 33 Type 1 with maximum stress criterion. Results at the end of the Step 2: in the left image is displacement (mm) of the laminated plate in the left image, in the right image is shown failure index (-) for element. 51

Fig. 34 Type 1 with Hill criterion. Results at the end of the Step 1: in the left image is displacement (mm) of the laminated plate in the left image, in the right image is shown failure index (-) for element. 52

Fig. 35 Type 1 with Hill criterion. Results at the end of the Step 2: in the left image is displacement (mm) of the laminated plate in the left image, in the right image is shown failure index (-) for element. 52

Fig. 36 Type 1 with Tsai-Wu criterion. Results at the end of the Step 1: in the left image is displacement (mm) of the laminated plate in the left image, in the right image is shown failure index (-) for element. 53

Fig. 37 Type 1 with Tsai-Wu criterion. Results at the end of the Step 2: in the left image is displacement (mm) of the laminated plate in the left image, in the right image is shown failure index (-) for element.* 53

Fig..38 Comparison of force-displacement curves and stiffnes-displacement curves of Type 2.* 54

Fig. 39 Type 2 with maximum stress criterion. Results at the end of the Step 1: in the left image is displacement (mm) of the laminated plate in the left image, in the right image is shown failure index (-) for element. 55

Fig. 40 Type 2 with maximum stress criterion. Results at the end of the Step 2: in the left image is displacement (mm) of the laminated plate in the left image, in the right image is shown failure index (-) for element. 55

Fig. 41 Type 2 with Hill criterion. Results at the end of the Step 1: in the left image is displacement (mm) of the laminated plate in the left image, in the right image is shown failure index (-) for element. 56

Fig. 42 Type 2 with Hill criterion. Results at the end of the Step 2: in the left image is displacement (mm) of the laminated plate in the left image, in the right image is shown failure index (-) for element. 56

Fig. 43 Type 2 with Tsai-Wu criterion. Results at the end of the Step 1: in the left image translational displacements (mm) of the laminated plate are shown, in the right image failure index (-) for element is shown. 57

Fig. 44 Type 2 with Tsai-Wu criterion. Results at the end of the Step 2: in the left image is displacement (mm) of the laminated plate in the left image, in the right image is shown failure index (-) for element.* 57

Fig. 45 Comparison of force-displacement curves on the left and stiffness-displacement curves on the right of Type 1 and Type 2 obtained by the measurement. 58

Fig. 46 Comparison of force-displacement curves on the left and stiffnes-displacement curves on the right of Type 1 an Type 2 obtained by FE analysis using maximum stress failure criterion. 58

Fig. 47 Comparison of force-displacement curves on the left and stiffnes-displacement curves on the right of Type 1 an Type 2 obtained by FE analysis using Hill failure criterion. 59

Fig. 48 Comparison of force-displacement curves on the left and stiffnes-displacement curves on the right of Type 1 an Type 2 obtained by FE analysis using Tsai-Wu failure criterion.* 59

Fig. 49 Determination of the ultimate load and ultimate displacement of Type 1 on the left and Type 2 on the right using Matlab from experimental data. 60

Fig. 50 Comparison of values of loads at ultimate displacement; Type 1 on the left, Type 2 on the right.* 61

Fig. 51 Comparison of loads F at displacement $u_z = 4$ mm of Type 1 in the left graph; comparison of loads F at displacement $u_z = 5{,}1$ mm of Type 2 in the right graph.* 61

List of tables

Table 1 Comparison of failure index and strength ratio. 28

Table 2 Comparison of capabilities of implicit and explicit solvers. 35

Table 3 Mesh sensitivity study. 38

Table 4 Material properties of one lamina of glass fiber reinforced polymer. 40

Table 5 Stacking sequence. 40

Table 6 Material properties of aluminium alloy D16. 41

Table 7 Materials properties for steel of the bolt. 41

Table 8 Material properties for steel of the reinforcement. 41

Table 9 List of contact used in model Type 1 44

Table 10 List of contact used in model Type 2. 44

Table 11 Geometrical properties of touched contact. 44

Table 12 Physical properties of touched contact. 45

Table 13 The loads used in the analyses. 48

Table 14 The values of ultimate displacements and loads obtained 60

Table 15 Summary of omitted entities and influences. 63